NATIONAL AERONAUTICS AND SPACE ADMINISTRATION

Technical Report 32-1528

Structural Analysis of Silicon Solar Arrays

L. W. Butterworth

R. K. Yasui

JET PROPULSION LABORATORY

CALIFORNIA INSTITUTE OF TECHNOLOGY

PASADENA, CALIFORNIA

May 15, 1971

NATIONAL AERONAUTICS AND SPACE ADMINISTRATION

Technical Report 32-1528

Structural Analysis of Silicon Solar Arrays

L. W. Butterworth

R. K. Yasui

JET PROPULSION LABORATORY

CALIFORNIA INSTITUTE OF TECHNOLOGY

PASADENA, CALIFORNIA

May 15, 1971

Preface

The work described in this report was performed by the Engineering Mechanics Division of the Jet Propulsion Laboratory.

Acknowledgment

Contents

Tables

Contents (contd)

Tables (contd)

Figures

Abstract

This report deals with the structural design of solar arrays. The different areas of examination include thermal stresses in array components, mechanical stresses in solar arrays, analysis of a stress relief interconnect, and current material properties. Special emphasis has been placed on developing simple but accurate methods of analysis that will be of use to the designer.

Structural Analysis of Silicon Solar Arrays

I. Introduction

This report deals with the structural design and testing of solar arrays. Its primary emphasis is on analytic methods necessary for the design of solar arrays, as this was determined to be the area of most critical need. The data available from present testing techniques is better than data available from the commonly used analytic methods. This fact has forced many solar cell companies to use a "shotgun" approach to design. Although this method usually produces a product that meets the required specifications, one does not know why the system works or how to improve it. It was the purpose of this project to collect and develop the necessary tools so that analytic design would be possible.

Most of the people who work with solar arrays are trained as electrical engineers rather than as mechanical or structural engineers. In view of this fact an effort has been made to explain the importance of the areas of concern and the causes of the major problems associated with each area. This approach should give the user a fundamental understanding of problem areas, which in turn should facilitate problem solution.

In this report, each main section is independent; one need not read the entire report to understand the part. Furthermore, variables in each equation are defined with the equation rather than in a separate table. This system is somewhat repetitive, but it should ease reference use. The analysis in each section has been developed as clearly as possible so that future investigators will know exactly what was done and what assumptions were made in order to arrive at each result.

This report is but a first step toward solving the structural problems of solar arrays. Solar cell and array manufacturers are becoming increasingly aware of the value of analytic design and are funding rigorous efforts in this area. Appendix A and B present details of a new program at JPL that covers much of the work not treated herein. Appendix C summarizes the results of a symposium on

solar cell interconnect design held at JPL in March 1970. The combination of the work from these different sources should greatly ease and improve the design of the large-scale solar arrays required in the next several years.

Numerical computations in this report were originally performed using the British units and were subsequently converted to the International System of Units for publication.

II. Thermal Stresses in Array Components

When a solar array is subjected to a thermal environment, thermal stresses are set up in the different layers due to differences in their thermal expansivities and to thermal gradients across the array. Because of a lack of a thermally insulating atmosphere in outer space, both the temperatures and the rate of temperature change are extreme. To design an optimum lightweight solar array, one must be able to determine by analysis how these conditions affect the array and its various components.

One of the major areas of concern in such a thermal stress analysis is the stress induced in each layer of the array. Since widely different materials are used in a single array, these stresses are potentially large. Thus a good method of analyzing these stresses is necessary to insure dependable service. The following methods fulfill this requirement and should aid the designer in improving solar array design.

The net strain approach has been used at JPL starting with the *Surveyor* design. This method is based on the fact that when an array consisting of several layers rigidly bonded together is heated or cooled it will come to some net equilibrium position (Fig. 1). This equilibrium position will be a weighted average of the equilibrium positions of each layer. The weighting functions are the modulus of elasticity and the thickness of each layer. Thus a thicker, stiffer layer will be more dominant than a thinner or more flexible layer. The equilibrium or net strain position is given by

$$\epsilon_{net} = \frac{\sum\limits_{i=1}^{N} h_i E_i \alpha_i \Delta T}{\sum\limits_{i=1}^{N} h_i E_i} \tag{1}$$

where h is the thickness, E is the modulus of elasticity, α is the coefficient of thermal expansion, ΔT is the change in
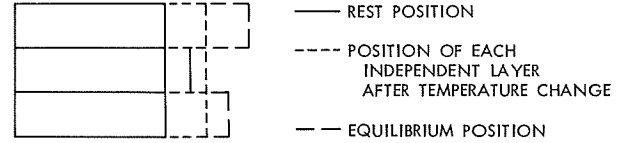
Fig. 1. Relative displacements in a three-layer composite subjected to temperature

temperature, and N is the number of layers. The stress in each layer is equal to

$$\sigma_i = (\epsilon_{net} - \alpha_i \Delta T) E_i \tag{2}$$

Typical results using this net strain approach are shown in Table 1. As a convenient check on this type of result, one may apply the condition that $\Sigma A_i \sigma_i = 0$. This condition comes directly from the force equilibrium equation and, as can be seen, it is satisfied by these results.

Table 1. Thermal stresses for silicon rigidly bonded to aluminum ($\Delta T = 38°C$)

h_{Si}, cm	h_{Al}, cm	σ_{Si}, N/cm^2	σ_{Al}, N/cm^2
0.013	0.254	11974.	−634.
0.025	0.254	11683.	−1163.
0.051	0.254	11102.	−2219.
0.013	0.127	11683.	−1163.
0.025	0.127	11102.	−2219.
0.051	0.127	10102.	−4037.
0.013	0.025	9661.	−4840.
0.025	0.025	7952.	−7947.
0.051	0.025	5870.	−11731.

$\alpha_{Si} = 2.88 \times 10^{-6}$ cm/cm/°C; $\alpha_{Al} = 21.6 \times 10^{-6}$ cm/cm/°C; $E_{Si} = 11.6 \times 10^{6}$ N/cm^2; $E_{Al} = 7.4 \times 10^{6}$ N/cm^2.

On examination of this method, one can see that it is only an approximation since it does not include bending or shear stresses. The effect of bending stresses due to the thermal loading can be taken into account fairly easily. As the following derivation (Ref. 1) will show, however, this bending redistributes the stress but does not change the maximum value.

The normal strains in the x direction (Fig. 2) can be written as

$$\epsilon_x(1) = \alpha_1 \Delta T + \frac{P}{E_1 t_1 b} - \frac{1}{\rho_1}\left(y - \frac{t_1}{2}\right) \tag{3a}$$

$$\epsilon_x(2) = \alpha_2 \Delta T - \frac{P}{E_2 t_2 b} - \frac{1}{\rho_2}\left(y - \frac{t_2}{2}\right) \tag{3b}$$

where

$$\frac{1}{\rho_i} = \frac{M}{E_i I_i} \tag{4}$$

E = modulus of elasticity

b = width

t = thickness

α = coefficient of thermal expansion

ΔT = temperature difference

I = cross-section moment of inertia

In Eqs. (3ab), the first term is the thermal expansion, the second term is the strain due to the normal force P, and the third term is the strain due to the bending moment.

Working now with Eq. (4), we obtain

$$\frac{1}{\rho_i} = \frac{M}{E_i I_i} = \frac{P t_i}{2 E_i \left(\frac{1}{12} b t_i^3 \right)} = \frac{6P}{E_i b t_i^2}$$

At $y = 0$, the strain in each layer must be equal for the layers to remain bonded. Therefore,

$$\alpha_1 \Delta T + \frac{P}{E_1 t_1 b} + \frac{t_1}{2\rho_1} = \alpha_2 \Delta T - \frac{P}{E_2 t_2 b} - \frac{t_2}{2\rho_2}$$
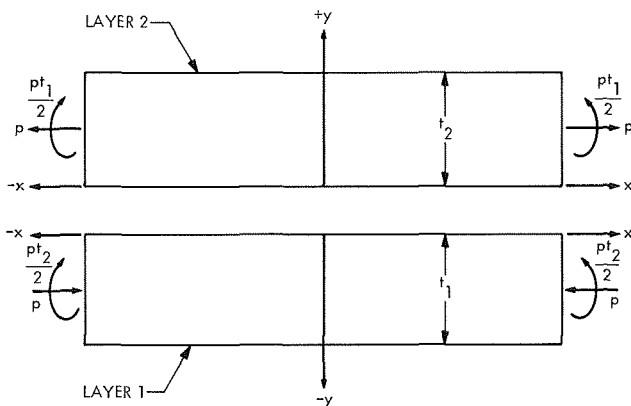
Fig. 2. Internal force distribution in a two-layer composite subjected to temperature

Now, substituting for $1/\rho_i$ in this equation and solving for P, we obtain

$$P \left(\frac{1}{E_1 t_1 b} + \frac{1}{E_2 t_2 b} \right) = (\alpha_2 - \alpha_1) \Delta T - 3P \left(\frac{1}{E_1 t_1 b} + \frac{1}{E_2 t_2 b} \right)$$

$$P = \frac{(\alpha_2 - \alpha_1) \Delta T}{4 \left(\frac{1}{E_1 t_1 b} + \frac{1}{E_2 t_2 b} \right)}$$

Now, substituting into Eq. (3a) at $y = 0$ gives

$$\epsilon_x(1) = \alpha_1 \Delta T + \frac{P}{E_1 t_1 b} + \frac{1}{\rho_1} \frac{t_1}{2}$$

$$\epsilon_x(1) = \alpha_1 \Delta T + \frac{(\alpha_2 - \alpha_1) \Delta T}{4 \left(\frac{1}{E_1 t_1 b} + \frac{1}{E_2 t_2 b} \right) E_1 t_1 b}$$

$$+ \frac{6 (\alpha_2 - \alpha_1) \Delta T \, t_1}{4 \left(\frac{1}{E_1 t_1 b} + \frac{1}{E_2 t_2 b} \right) 2 E_1 t_1^2 b}$$

Simplifying and collecting terms gives

$$\epsilon_x(1) = \alpha_1 \Delta T + \frac{(\alpha_2 - \alpha_1) \Delta T (1 + 3)}{4 \left(\frac{1}{E_1 t_1 b} + \frac{1}{E_2 t_2 b} \right) E_1 t_1 b}$$

$$= \alpha_1 \Delta T + \frac{(\alpha_2 - \alpha_1) \Delta T}{\left(\frac{1}{E_1 t_1 b} + \frac{1}{E_2 t_2 b} \right) E_1 t_1 b}$$

$$= \alpha_1 \Delta T + \frac{(\alpha_2 - \alpha_1) \Delta T}{\left(1 + \frac{E_1 t_1 b}{E_2 t_2 b} \right)}$$

$$= \frac{\left(1 + \frac{E_1 t_1 b}{E_2 t_2 b} \right) \alpha_1 \Delta T}{\left(1 + \frac{E_1 t_1 b}{E_2 t_2 b} \right)} + \frac{(\alpha_2 - \alpha_1) \Delta T}{\left(1 + \frac{E_1 t_1 b}{E_2 t_2 b} \right)}$$

Multiplying through and rearranging terms gives

$$\epsilon_x(1) = \frac{E_1 t_1 b \, \alpha_1 \Delta T + E_2 t_2 b \, \alpha_2 \Delta T}{E_1 t_1 b + E_2 t_2 b}$$

This is exactly the same result as the net strain approach. For verification that maximum stress does not change and is at the bondline in this case see Ref. 2, page 357.

One should remember that for this type of work the principle of superposition holds and bending stresses can simply be added to the thermal stresses. Thus, if one wants detailed stress distributions, the methods developed in the section on mechanical stresses can be used to get the bending stresses in a complicated array.

This analysis still does not take into account shear stress, which is extremely important if the middle layer of a laminate is much more flexible than the outer two. In this case, the middle layer will be deformed in shear, and the edges of the different layers will no longer line up. For this case the net strain approach was not valid, and a new method of analysis had to be developed.

Much time was spent developing and refining methods to account for the shear stress in the bond material. The first method was an iterative technique involving the integration of the bond shear stress to determine the resulting normal strains in the outer layers. An attempt was made to generalize this procedure, but it was unsuccessful. By applying additional boundary conditions, the iterative solution was converted to a closed form solution. This solution did not take into account nonlinear shear stress distributions, and several of the basic assumptions oversimplified the problem. The latest work, which is presented here, uses strain energy techniques and is far better than the previous work. It takes into account nonlinear shear stress distributions and can be modified fairly easily to include practically any phenomena. The basic model for this method is shown in Fig. 3, where the equation parameters are defined.

Certain assumptions were made to simplify the problem of calculating the required strains and shear stresses. The three basic assumptions made were:

(1) The elastic moduli of the outside layers are much larger than the elastic moduli of the bond material.

(2) The thickness of the bond is small.

(3) The overall laminate thickness is much smaller than the length of the cell.

These assumptions were obviously valid for the type of solar cell configurations under investigation and permitted the following simplifying approximations:

(1) The σ_x is uniform across the thickness of the outside layers.
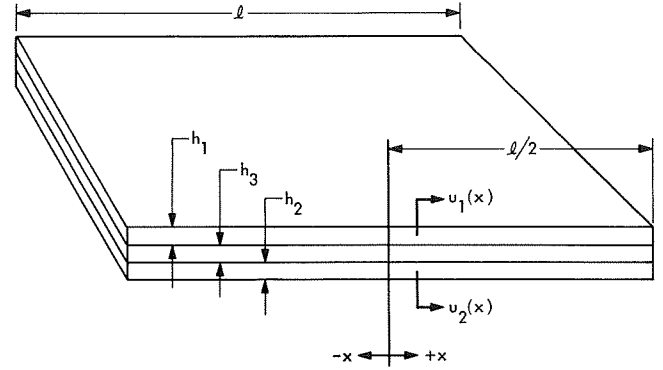
Fig. 3. Basic model of three laminated layers

(2) The τ_{xy} in the outside layers does not produce appreciable strain.

(3) The σ_x in the bond material is small compared to the σ_x in the outside layer and can be neglected in the calculation of the normal strains in the outside layers.

In Fig. 3, the shear stress in layer 3 is taken as

$$\tau = \frac{G_3}{h_3}(u_2 - u_1)$$

For a unit width section, the normal stresses in layers (1) and (2) are

$$\sigma_x(1) = E_1 \frac{du_1}{dx} - E_1 \alpha \Delta T$$

$$\sigma_x(2) = E_2 \frac{du_2}{dx} - E_2 \alpha \Delta T$$

respectively.

Thus the strain energy stored in the material is

$$U = \int_{-l/2}^{l/2} \left\{ \left[\frac{1}{2} E_1 h_1 (u_1')^2 + \frac{1}{2} E_2 h_2 (u_2')^2 \right. \right.$$

$$\left. + \frac{1}{2} \frac{G_3}{h_3} (u_1 - u_2)^2 \right] - \alpha_1 E_1 h_1 \Delta T \frac{du_1}{dx}$$

$$\left. - \alpha_2 E_2 h_2 \Delta T \frac{du_2}{dx} \right\} dx$$

If the outer plates incur a virtual displacement δu_i, the material change in the strain energy will be

$$\delta U = \int_{-l/2}^{l/2} \left[E_1 h_1 u_1' \delta u_1' + E_2 h_2 u_2' \delta u_2' \right.$$
$$\left. + \frac{G_3}{h_3} (u_1 - u_2)(\delta u_1 - \delta u_2) \right] dx$$

This virtual displacement causes work to be done such that

$$\delta W = \sigma_x(1) A(1) \left. \frac{du_1}{dx} \right|_{x=-l/2} + \sigma_x(2) A(2) \left. \frac{du_2}{dx} \right|_{x=l/2}$$

The principle of virtual work requires that

$$\delta U = \delta W$$

Setting the two equations equal, integrating by parts, and collecting terms, one obtains the following equation.

$$\int_{-l/2}^{l/2} \left\{ \left[-E_1 h_1 u_1'' + \frac{G_3}{h_3}(u_1 - u_2) \right] \delta u_1 \right.$$
$$\left. + \left[-E_2 h_2 u_2'' + \frac{G_3}{h_3}(u_2 - u_1) \right] \delta u_2 \right\} dx = 0$$

Since δu_1 is independent of δu_2, each expression within the integral must be equal to zero. Thus one obtains the following two equations:

$$E_1 h_1 u_1'' - \frac{G_3}{h_3}(u_1 - u_2) = 0 \tag{5}$$

$$E_2 h_2 u_2'' - \frac{G_3}{h_3}(u_2 - u_1) = 0 \tag{6}$$

As a check on the validity of these equations, one can derive them from the equilibrium equation. Taking a piece of material of unit width and length and h units high, one has the situation shown as follows:
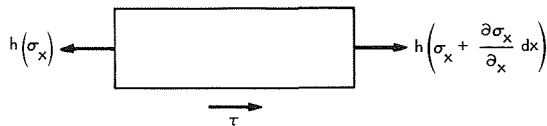
Summing forces, one obtains

$$h \frac{\partial \sigma_x}{\partial x} + \tau = 0 \tag{7}$$

But σ_x and τ were previously defined as

$$\sigma_x(1) = E_1 \frac{du_1}{dx} - E_1 \alpha_1 \Delta T$$

$$\tau = \frac{G_3}{h_3}(u_2 - u_1)$$

Substituting these values into Eq. (7) one obtains

$$Eh \frac{d^2 u}{dx^2} - \alpha \frac{\partial \Delta T}{\partial x} Eh + \frac{G_3}{h_3}(u_2 - u_1) = 0$$

Since $\partial \Delta T / \partial x$ is taken to be zero in this case, one obtains the same result as from the energy solution.

The solution to Eqs. (5) and (6) will be of the form $Ae^{\lambda x}$. Writing the equations in matrix form, one obtains

$$\begin{bmatrix} \lambda^2 - K_1 & K_1 \\ K_2 & \lambda^2 - K_2 \end{bmatrix} \begin{bmatrix} Ae^{\lambda x} \\ Be^{\lambda x} \end{bmatrix} = 0$$

where

$$K_1 = \frac{G_3}{h_3 E_1 h_1}$$

$$K_2 = \frac{G_3}{h_3 E_2 h_2}$$

The characteristic equation is obtained by setting the determinant of the first matrix equal to zero. Thus,

$$(\lambda^2 - K_1)(\lambda^2 - K_2) - K_1 K_2 = 0$$

or

$$\lambda^4 - \lambda^2 (K_1 + K_2) = 0$$

The roots of this equation are $0, 0, \pm \sqrt{K_1 + K_2}$. Letting $2\beta = \sqrt{K_1 + K_2}$ and using hyperbolic functions rather than expotential functions, one finds the solutions to Eqs. (5) and (6) to be

$$u_1 = A_1 + A_2 x + A_3 \sinh 2\beta x + A_4 \cosh 2\beta x \tag{8}$$

$$u_2 = B_1 + B_2 x + B_3 \sinh 2\beta x + B_4 \cosh 2\beta x \tag{9}$$

Since the stresses, which depend on u_i, are symmetric about $x = 0$, A_4 and B_4 must equal zero. In addition, the displacement must be zero at $x = 0$. Thus A_1 and B_1 must

also equal zero. When these values of u_1 and u_2 are substituted into Eq. (5), the equation becomes

$$[4A_3\beta^2 \sinh 2\beta x - K_1(A_3 - B_3) \sinh 2\beta x]$$
$$- [K_1(A_2 - B_2)x] = 0$$

Since this equation must be valid for all x between $-l/2$ and $+l/2$, the terms in each bracket must equal zero separately. This implies that $A_2 = B_2$ and that $K_1 B_3 = A_3[K_1 - 4\beta^2]$. Remembering that $2\beta = \sqrt{K_1 + K_2}$, one finds the second condition to be

$$B_3 = -\frac{K_2}{K_1}A_3$$

Equations (8) and (9) now become

$$u_1 = A_2 x + A_3 \sinh 2\beta x \qquad (10)$$

$$u_2 = A_2 x - \frac{K_2}{K_1} A_3 \sinh 2\beta x \qquad (11)$$

The A_2 and A_3 can now be determined using the boundary conditions that

$$h_1 \sigma_x(1)\big|_{x=l/2} = 0$$

$$h_2 \sigma_x(2)\big|_{x=l/2} = 0$$

Substituting for σ_x in these equations, one obtains

$$E_1 h_1 \frac{du_1}{dx} - E_1 h_1 \alpha_1 \Delta T = 0$$

$$E_2 h_2 \frac{du_2}{dx} - E_2 h_2 \alpha_2 \Delta T = 0$$

By substituting the values of u_1 and u_2 from Eqs. (10) and (11) into these equations, the values of A_2 and A_3 can be determined to be

$$A_2 = \frac{\dfrac{K_2}{K_1}\alpha_1 \Delta T + \alpha_2 \Delta T}{1 + \dfrac{K_2}{K_1}}$$

$$A_3 = \frac{\alpha_1 \Delta T - \alpha_2 \Delta T}{\left(1 + \dfrac{K_2}{K_1}\right)2\beta \cosh \beta l}$$

Remembering the definitions of K_1 and K_2, one finds these values of A_2 and A_3 can be substituted into Eqs. (10) and (11) to obtain the displacements in the following form.

$$u_1 = \frac{(E_1 h_1 \alpha_1 \Delta T + E_2 h_2 \alpha_2 \Delta T)x}{E_1 h_1 + E_2 h_2}$$
$$+ \frac{E_2 h_2 (\alpha_1 \Delta T - \alpha_2 \Delta T)\sinh 2\beta x}{(E_1 h_1 + E_2 h_2)2\beta \cosh \beta l}$$

$$u_2 = \frac{(E_1 h_1 \alpha_1 \Delta T + E_2 h_2 \alpha_2 \Delta T)x}{E_1 h_1 + E_2 h_2}$$
$$- \frac{E_1 h_1 (\alpha_1 \Delta T - \alpha_2 \Delta T)\sinh 2\beta x}{(E_1 h_1 + E_2 h_2)2\beta \cosh \beta l}$$

At the beginning of this derivation, σ_x and τ_{xy} were given in terms of u_1 and u_2 as

$$\sigma_x(1) = E_1\left(\frac{du_1}{dx} - \alpha_1 \Delta T\right)$$

$$\sigma_x(2) = E_2\left(\frac{du_2}{dx} - \alpha_2 \Delta T\right)$$

$$\tau_{xy} = \frac{G_3}{h_3}(u_2 - u_1)$$

Substituting the value of u_1 and u_2 into these equations one obtains

$$\sigma_x(1) = E_1\left[\frac{E_1 h_1 \alpha_1 \Delta T + E_2 h_2 \alpha_2 \Delta T}{E_1 h_1 + E_2 h_2}\right.$$
$$\left. + \frac{E_2 h_2 (\alpha_1 \Delta T - \alpha_2 \Delta T)\cosh 2\beta x}{(E_1 h_1 + E_2 h_2)\cosh \beta l} - \alpha_1 \Delta T\right]$$

$$\sigma_x(2) = E_2\left[\frac{E_1 h_1 \alpha_1 \Delta T + E_2 h_2 \alpha_2 \Delta T}{E_1 h_1 + E_2 h_2}\right.$$
$$\left. - \frac{E_1 h_1 (\alpha_1 \Delta T - \alpha_2 \Delta T)\cosh 2\beta x}{(E_1 h_1 + E_2 h_2)\cosh \beta l} - \alpha_2 \Delta T\right]$$

$$\tau_{xy} = \frac{G_3 (\alpha_2 \Delta T - \alpha_1 \Delta T)\sinh 2\beta x}{h_3 2\beta \cosh \beta l}$$

In each of these equations β is defined as

$$\beta = \frac{1}{2}\sqrt{\frac{G_3}{h_3}\left[\frac{1}{E_1 h_1} + \frac{1}{E_2 h_2}\right]}$$

By looking at the equations for the normal stresses one can see that the first and third terms are the same as the

net strain approach, and that the second term involves the bond layer.

As a quick check on the validity of these equations, the case where $\alpha_1 \Delta T = \alpha_2 \Delta T$ can be analyzed. As would be expected,

$$u_1 = u_2 = \alpha \Delta T; \qquad \sigma_x(1) = \sigma_x(2) = \tau_{xy} = 0$$

Throughout this work, ΔT has been assumed to be the same for both outer layers. This was done for simplicity and is not necessary to the equation. Different ΔTs can be used to account for thermal gradient across the thickness of the array.

These equations were used to determine the stresses in array configurations. The results are given in Table 2. As would be expected, thinner and stiffer bond layers cause increased stresses in the substrate and cell. In the limiting case of no bond thickness or a completely rigid bond, the stress is the same as that calculated using the net strain approach.

Table 2. Thermal stresses for silicon flexibly bonded to aluminum ($\Delta T = 38°C$)

G_{bond}, N/cm^2	h_{bond}, cm	h_{Si}, cm	h_{Al}, cm	σ_{Si}, N/cm^2	σ_{Al}, N/cm^2
1409	0.005	0.025	0.025	2826	−2826
1409	0.010	0.025	0.025	1906	−1906
1409	0.015	0.025	0.025	1420	−1420
2818	0.005	0.025	0.025	3681	−3681
2818	0.010	0.025	0.025	2826	−2826
2818	0.015	0.025	0.025	2253	−2253
1409	0.005	0.013	0.025	4069	−2035
1409	0.010	0.013	0.025	2745	−1372
1409	0.015	0.013	0.025	2045	−1022
2818	0.005	0.013	0.025	5331	−2665
2818	0.010	0.013	0.025	4069	−2035
2818	0.015	0.013	0.025	3246	−1623
7045	0.005	0.013	0.025	6366	3182
7045	0.010	0.013	0.025	5644	2822
7045	0.015	0.013	0.025	4988	2494

$\alpha_{Si} = 2.88 \times 10^{-6}$ cm/cm/°C; $\alpha_{Al} = 21.6 \times 10^{-6} \times 10^{-6}$ cm/cm/°C; $E_{Si} = 11.6 \times 10^{6}$ N/cm^2; $E_{Al} = 7.4 \times 10^{6}$ N/cm^2.

For a given set of environmental conditions, the use of thinner cells with the same substrate and bond will cause an increase in cell stress level.

As was stated earlier, this method can be expanded to include additional conditions such as bending stiffness, plate action, and so forth. These conditions will increase the complexity of the problem and may make the solution too cumbersome to be used effectively. These matters did not receive appropriate attention because of a lack of time and possibly should be studied further.

One addition that seems acceptable but has not been verified, is the inclusion of the thermal activity of the bond layer in the first term of the displacement and stress equations. It should be included in exactly the same manner as the thermal activity of the other layers. As was said, this addition has not been fully derived but seems acceptable at this time.

III. Mechanical Stresses in Solar Arrays

In addition to the loadings caused by the thermal environment, the solar array is also loaded by the inertial forces due to the launch acceleration and by the flexing of the array due to vibration during launch. After burnout, these conditions are no longer present, but during the launch period they may become very pronounced. It is thus important to analyze these two problems to determine how significant they are in the overall array design.

A. Bending Stresses Due to Vibration

When a rigid array vibrates, it bends the cells attached to it, causing stresses in these cells. These stresses are a function of the curvature of the cell; thus, knowing the maximum curvature, one can easily determine the maximum stresses using well-known formulas.

In Figs. 4 and 5, the results of modal tests on the *Mariner* 1969 panel are shown. Since the maximum curvature occurs in the results shown in Fig. 5, this data will be used to determine the stresses. The displacements are summarized in Table 3 for convenience.

Table 3. Displacements of *Mariner* Mars 1969 panel during modal testing

Distance from panel center, cm	Displacement from rest position, cm
−38.735	+0.188
−25.908	+0.099
−13.030	+0.033
0.00	0.00
+13.030	+0.033
+25.908	+0.099
+38.735	+0.188

Using this data one must determine the maximum curvature of the panel to determine the maximum stress.
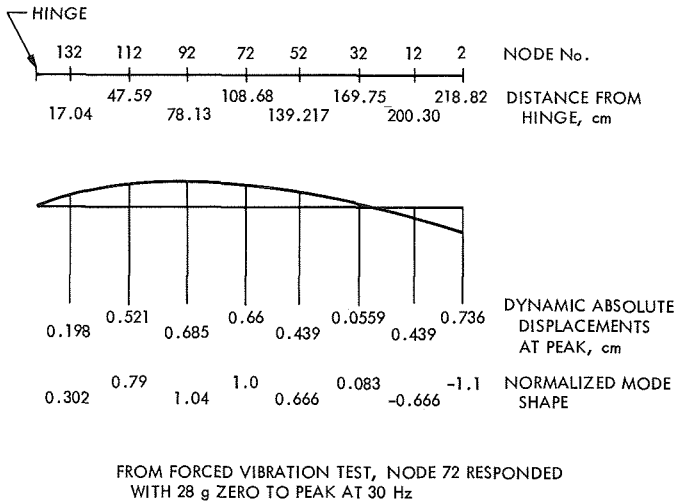
Fig. 4. Side view of Mariner Mars 1969 panel

HINGE

NODE No.: 132 112 92 72 52 32 12 2

DISTANCE FROM HINGE, cm: 17.04 47.59 78.13 108.68 139.217 169.75 200.30 218.82

DYNAMIC ABSOLUTE DISPLACEMENTS AT PEAK, cm: 0.198 0.521 0.685 0.66 0.439 0.0559 0.439 0.736

NORMALIZED MODE SHAPE: 0.302 0.79 1.04 1.0 0.666 0.083 -0.666 -1.1

FROM FORCED VIBRATION TEST, NODE 72 RESPONDED WITH 28 g ZERO TO PEAK AT 30 Hz

Fig. 5. End view of Mariner Mars 1969 panel

DISTANCE FROM CENTERLINE, cm: -38.755 -25.90 -13.03 13.03 25.90 38.735

DYNAMIC ABSOLUTE DISPLACEMENTS AT PEAK, cm: -0.104 -0.0152 0.0508 0.0838 0.0508 -0.0152 -0.104

NORMALIZED MODE SHAPE: -1.23 -0.192 0.615 1.0 0.615 -0.192 -1.23

Now assume that the displacement can be written as a function of the distance from the center of the panel. Thus, $v = f(x)$. Assuming that the displacement can be written as a polynomial, $v(x)$ will have the following form:

$$v(x) = ax^6 + bx^4 + cx^2 + dx^5 + ex^3 + fx + g$$

Since at $x = 0$, $v(x) = 0$, g must equal zero. Since the displacement is symmetric about the origin, $v(x)$ can have only even powers of x. Thus $d = e = f = 0$, and $v(x)$ becomes

$$v(x) = ax^6 + bx^4 + cx^2 \qquad (12)$$

The maximum curvature is at the center of the panel, and this curvature may be written in terms of the first and second derivatives of the displacement.

$$\text{Curvature} = \frac{\dfrac{d^2v}{dx^2}}{\left[1 + \left(\dfrac{d_v}{dx}\right)^2\right]^{3/2}} \qquad (13)$$

$$v(x) = ax^6 + bx^4 + cx^2$$

$$\frac{d_v}{dx} = 6ax^5 + 4bx^3 + 2cx$$

$$\frac{d^2v}{dx^2} = 30ax^4 + 12bx^2 + 2c$$

Evaluating these derivatives at $x = 0$, one obtains

$$\frac{d_v}{dx} = 0$$

$$\frac{d^2v}{dx^2} = 2c$$

Substituting these values into Eq. (13) determines the curvature of the panel at $x = 0$.

$$\text{Curvature} = \frac{2c}{[1 + (0)^2]^{3/2}} = 2c$$

To determine c, Eq. (12) must be solved at three different points simultaneously. Since $x = 0$ was used to eliminate a constant from the original equation and one of each pair of symmetric points was used to prove symmetry and eliminate the odd powers of x, the three remaining values of x are: $x = 5.13$, 10.20, and 15.25. Substituting each of these values into Eq. (12), and solving the three equations simultaneously, one obtains, $c = 1.45 \times 10^{-3}$. Since the curvature is equal to $2c$, the curvature equals 1.14×10^{-3} 1/cm.

The inverse of the curvature is called the radius of curvature. Thus in this case the radius of curvature is $R = 1/2.9 \times 10^{-3} = 876.3$ m. The bending moment M required to achieve a radius of curvature R in a given body is $M = EI/R$, where E is the modulus of elasticity and I is the moment of inertia of the body's cross section.

For single curvature bending in a plate the stress is

$$\sigma = \frac{My}{I(1 - v^2)}$$

where y is the distance from the neutral axis and v is Poisson's ratio. Substituting for M in this equation one obtains,

$$\sigma = \frac{Ey}{R(1 - v^2)}$$

Since the neutral axis is usually in the middle of the plate, y_{max} is usually equal to one-half the cell thickness. Thus the maximum stress is

$$\sigma_{max} = \frac{Eh}{2R(1 - v^2)}$$

For a 0.0254-cm cell with $E = 11.6 \times 10^6$ N/cm^2 and $v = 0.3$, the maximum stress will be about 190.2 N/cm^2.

B. Stresses and Deflections Due to Inertia Loadings

Since the present trend is toward lighter and lighter solar arrays, the mass of the cell and its interconnectors is becoming a significant portion of the overall mass. As this trend continues, inertia loadings due to launch conditions may become significant enough to cause cell and inter-connector failure.

The total force acting on a cell due to inertia is simply $F = m \cdot a$; the mass of the cell is its weight in Newtons divided by 980.9 cm/sec^2. Maximum accelerations of rigid arrays typically run between 30 and 35 g. Thus the total force acting on the cell is equal to

$$F = (\text{volume})\,(\text{density})/980.9 \text{ cm/s}^2$$
$$\times (\text{number of } g) \times 980.9 \text{ cm/s}^2$$

or

$$F = \text{volume} \times \text{density} \times \text{number of } g$$

Since the mass of the cell is uniformly distributed for all practical purposes, the force is also uniformly distributed. The normal loading on a cell is then

$$P = F/A = (\text{cell thickness}) \times (\text{density of silicon})$$
$$\times (\text{number of } g)$$

The density of silicon is 0.002 Kg/cm^3; thus a 0.0254-cm cell subjected to 30 g would feel a normal force of

1.76 $\times$ 10^{-2} N/cm^2. This loading is exceedingly small, so inertia loadings are not a major factor in panel design.

If one is interested in the deflection caused by inertial loading, Timoshenko gives the following formulas and constants in *Theory of Plates and Shells* (Ref. 3).

$$\text{Deflection} = \frac{\alpha q a^4}{D}$$

where

$\alpha = $ constant obtained from Tables 4–6 (from Ref. 3)

$q = $ load/unit area, N/cm^2

$a = $ length of side in x direction, cm

$D = $ flexual rigidity

$$= \frac{Eh^3}{12(1 - v^2)}, \text{N/cm}$$

The stress caused by this deflection can be calculated from

$$\sigma_x = \frac{EZ}{1 - v^2} \frac{d^2w}{dx^2}$$

but

$$D\frac{d^2w}{dx^2} = -M$$

$$\sigma_x = \frac{-EZ}{1 - v^2} \frac{M}{D}$$

Now, $Z = h/2$ and $D = Eh^3/(1 - v^2)$. Thus by substitution,

$$\sigma_x = \frac{6M}{h^2}$$

The bending moment M can be found from the given tables. For a 0.0254-cm cell undergoing a 30-g loading, the maximum stress is 95.1 N/cm^2.

When a cell is subjected to single-curvature bending, the constants of Table 4 should be used to calculate the stresses and displacements.

$\dfrac{b}{a}$	$x = \dfrac{a}{2}, y = 0$			$x = \dfrac{a}{2}, y = \pm\dfrac{b}{2}$	
	$w = \alpha \dfrac{qa^4}{D}$	$M_x = \beta_1 qa^2$	$M_y = \beta_1' qa^2$	$w = \alpha_2 \dfrac{qa^4}{D}$	$M_x = \beta_2 qa^2$
	α_1	β_1	β_1'	α_2	β_2
0.5	0.01377	0.1235	0.0102	0.01443	0.1259
1.0	0.01309	0.1225	0.0271	0.01509	0.1318
2.0	0.01289	0.1235	0.0364	0.01521	0.1329
∞	0.01302	0.1250	0.0375	0.01522	0.1330

Similarly, when a cell is subjected to double-curvature bending, the constants of Table 5 should be used. Table 6 gives the constants for intermediate edge conditions.

IV. Analysis of Stress Relief Interconnects

There has been considerable work done in the area of stress relief loop interconnect design. Most of this work has been based on straight beam theory, which often does not adequately represent the true situation in the curved interconnect. The following analysis is based on curved beam theory and relates displacements between cells to stresses in the interconnect.

The reason that straight beam theory is inadequate for curved beams is that in a curved beam the neutral axis is not coincident with the centroidal axis. The neutral axis is shifted toward the center of curvature, thus changing the stress distribution. The bending stress at a point y units from the centroidal axis is given by the formula

$$\sigma = \frac{M}{AR}\left[1 + \frac{y}{Z(R + y)}\right] \tag{14}$$

where M is the applied bending moment, A is the cross sectional area, R is the radius of curvature, and Z is a property of the cross section, which is defined by

$$Z = -\frac{1}{A}\int \frac{y}{R + y}\, dA \tag{15}$$

This integration may become a bit cumbersome, so the value of Z for standard cross sections is usually tabulated in standard mechanical engineering handbooks (Ref. 4). The values for typical interconnect cross sections are given in Table 7 (from Ref. 4).

To insure proper stress definition, the following sign conventions should be followed. The bending moment M should be given a positive sign when it acts to decrease the radius of curvature and a negative sign when it acts to increase the radius of curvature. The distance y should be positive when measured away from the center of curvature and negative when measured toward the center of curvature.
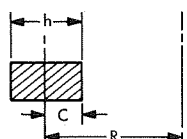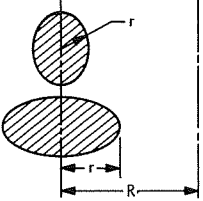
$\dfrac{b}{a}$	$w_{max} = \alpha \dfrac{qa^4}{D}$	$(M_x)_{max} = \beta qa^2$	$(M_y)_{max} = \beta_1 qa^2$	$(Q_x)_{max} = \gamma qa$	$(Q_y)_{max} = \gamma_1 qa$	$(V_x)_{max} = \delta qa$	$(V_y)_{max} = \delta_1 qa$	$R = nqa^2$
	α	β	β_1	γ	γ_1	δ	δ_1	n
1.0	0.00406	0.0479	0.0479	0.338	0.338	0.420	0.420	0.065
1.1	0.00485	0.0554	0.0493	0.360	0.347	0.440	0.440	0.070
1.2	0.00564	0.0627	0.0501	0.380	0.353	0.455	0.453	0.074
1.3	0.00638	0.0694	0.0503	0.397	0.357	0.468	0.464	0.079
1.4	0.00705	0.0755	0.0502	0.411	0.361	0.478	0.471	0.083
1.5	0.00772	0.0812	0.0498	0.424	0.363	0.486	0.480	0.085
1.6	0.00830	0.0862	0.0492	0.435	0.365	0.491	0.485	0.086
1.7	0.00883	0.0908	0.0486	0.444	0.367	0.496	0.488	0.088
1.8	0.00931	0.0948	0.0479	0.452	0.368	0.499	0.491	0.090
1.9	0.00974	0.0985	0.0471	0.459	0.369	0.502	0.494	0.091
2.0	0.01013	0.1017	0.0464	0.465	0.370	0.503	0.496	0.092
3.0	0.01223	0.1189	0.0406	0.493	0.372	0.505	0.498	0.093
4.0	0.01282	0.1235	0.0384	0.498	0.372	0.502	0.500	0.094
5.0	0.01297	0.1246	0.0375	0.500	0.372	0.501	0.500	0.095
∞	0.01302	0.1250	0.0375	0.500	0.372	0.500	0.500	0.095

Table 6. Deflections and bending moments at the center of a uniformly loaded square plate with two edges simply supported and the other two supported by elastic beams ($v = 0.3$)

$\lambda = \dfrac{EI}{aD}$	w_{max}	$(M_x)_{max}$	$(M_y)_{max}$
∞	$0.00406qa^4/D$	$0.0479qa^2$	$0.0479qa^2$
100	$0.00409qa^4/D$	$0.0481qa^2$	$0.0477qa^2$
30	$0.00416qa^4/D$	$0.0486qa^2$	$0.0473qa^2$
10	$0.00434qa^4/D$	$0.0500qa^2$	$0.0465qa^2$
6	$0.00454qa^4/D$	$0.0514qa^2$	$0.0455qa^2$
4	$0.00472qa^4/D$	$0.0528qa^2$	$0.0447qa^2$
2	$0.00529qa^4/D$	$0.0571qa^2$	$0.0419qa^2$
1	$0.00624qa^4/D$	$0.0643qa^2$	$0.0376qa^2$
0.5	$0.00756qa^4/D$	$0.0744qa^2$	$0.0315qa^2$
0	$0.01309qa^4/D$	$0.1225qa^2$	$0.0271qa^2$

Table 7. Analytical expressions for Z

SECTION	EXPRESSION
	$Z = -1 + \dfrac{R}{h}\left(\ln \dfrac{R+C}{R-C} \right)$
	$Z = -1 + 2\left(\dfrac{R}{r}\right)\left[\dfrac{R}{r} - \sqrt{\left(\dfrac{R}{r}\right)^2 - 1}\right]$
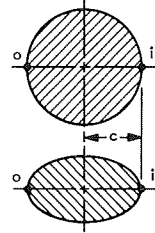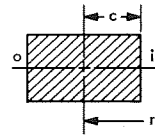
In order to further simplify these stress calculations, one may use straight beam theory and apply a correction factor. This method would serve well in the initial design stages where the design is likely to be changed often. The final design could be checked by using the full equations. The corrected equation is

$$\sigma = \frac{KMy}{I} \qquad (16)$$

where I is the moment of inertia of the cross section. The constant K is tabulated for the common cross sections in Table 8 (from Ref. 5).

One must also remember to add the direct stresses to the bending stresses calculated above. It is usually sufficient to assume a uniform stress distribution, thus making

Table 8. Stress factors for curved beams

$r/c \longrightarrow$	1.2	1.4	1.6	1.8	2.0	3.0	4.0
	6.0	8.0	10.0				
K_{ci}	3.41	2.40	1.96	1.75	1.62	1.33	1.23
	1.14	1.10	1.08				
K_{co}	0.54	0.60	0.65	0.68	0.71	0.79	0.84
	0.89	0.91	0.93				
K_{ci}	2.89	2.13	1.79	1.63	1.52	1.3	1.2
	1.12	1.09	1.07				
K_{co}	0.57	0.63	0.67	0.70	0.73	0.81	0.85
	0.9	0.92	0.94				

the overall stress equation in terms of the applied force equal to

$$\sigma = \frac{FL}{AR}\left[1 + \frac{y}{Z(R+y)} \right] + \frac{F}{A} \qquad (17)$$

Using the corrected straight beam equations, one obtains

$$\sigma = \frac{KFL}{I}y + \frac{F}{A} \qquad (18)$$

In both equations, L is the distance from the point of application of F to the centroidal axis of the curved section. Looking at a typical interconnect as shown in Fig. 6, one can see that L is equal to $l + R$.

The above equations are not immediately applicable because one does not usually know the force applied to the interconnect. Usually one is given, or can find, the displacement at the base of the interconnect, since this is the intercell spacing change. The relationship between the displacement and the applied force can easily be determined using Castigliano's theorem.
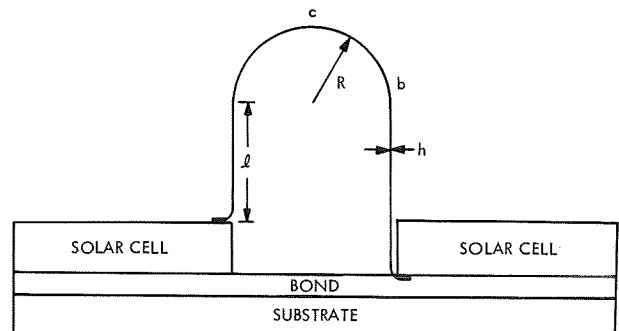
Fig. 6. Typical interconnect

Castigliano's theorem states that in an elastic system the displacement in the direction of a force or couple due to that force or couple is the partial derivative of the strain energy with respect to that force or couple. Thus

$$\delta = \frac{\partial U}{\partial F} \tag{19}$$

The strain energy in a beam is equal to

$$U = \int_0^s \frac{M^2 ds}{2EI} \tag{20}$$

Looking first at the straight section from a to b, one obtains

$$U = \int_0^l \frac{(Fx)^2}{2EI} dx$$

In the curved section from b to c there are two bending moments. One, due to the moment applied through l, is constant and equal to Fl. The second moment, due to the force F itself, varies along the interconnect and is equal to $FR \sin \theta$. Thus the strain energy in the curved section is equal to

$$U = \int_0^s \frac{(Fl + FR \sin \theta)^2}{2EI} ds$$

Now substituting $Rd\theta$ for ds and changing the limits of integration appropriately, the strain energy in the curved section from b to c is equal to

$$U = \int_0^{\pi/2} \frac{(Fl + FR \sin \theta)^2}{2EI} Rd\theta$$

Adding the strain energy stored in the straight segment of the interconnect, one obtains the strain energy stored in one-half the interconnect. Now realizing that the interconnect is symmetric, one can double this strain energy and obtain the total strain energy stored in the interconnect. Thus

$$U_{total} = 2 \left[\int_0^l \frac{(Fx)^2}{2EI} dx + \int_0^{\pi/2} \frac{(Fl + FR \sin \theta)^2 Rd\theta}{2EI} \right] \tag{21}$$

Taking the partial derivative of this equation with respect to F and carrying out the necessary integrations, one obtains

$$\frac{\partial U}{\partial F} = \delta = \frac{2F}{EI} \left[\frac{l^3}{3} + R \left(\frac{\pi}{2} l^2 + 2lR + \frac{\pi}{4} R^2 \right) \right] \tag{22}$$

Rearranging terms to obtain F yields

$$F = \frac{\delta EI}{2 \left[\frac{l^3}{3} + R \left(\frac{\pi}{2} l^2 + 2lR + \frac{\pi}{4} R^2 \right) \right]} \tag{23}$$

Equation (23) gives the force F in terms of the intercell spacing change δ and the physical properties of the interconnect. This value of F may now be substituted into Eq. (17) or (18) to obtain the induced stress. The complete equation is

$$\sigma = \left\{ \frac{L}{AR} \left[1 + \frac{y}{Z(R+y)} \right] + \frac{1}{A} \right\} \frac{\delta EI}{2 \left[\frac{l^3}{3} + R \left(\frac{\pi}{2} l^2 + 2lR + \frac{\pi}{4} R^2 \right) \right]} \tag{24}$$

If an interconnect has a rectangular cross section, it is easy to determine how to proportion the cross section in order to reduce the stress. The only terms in Eq. (24) that are affected by the cross section are the area and the moment of inertia. In this case the important parameter is the ratio I/A. If the cross section is b units wide and h units high, the area and moment of inertia are bh and $bh^3/12$, respectively. The critical ratio is thus $h^2/12$. Therefore, in order to reduce the stress, h must be as small as possible. Since b does not enter the critical ratio, the interconnect can be as wide as necessary to give sufficient cross-sectional area for low electrical resistance. If the interconnect is extremely wide it may begin to act as a plate rather than as a beam. This would increase the stress by approximately 9%, but it is highly unlikely that interconnects will be made this wide. In general, then, the trend toward thinner, wider interconnects reduces the maximum stress and hence improves the design.

If there is a maximum allowable height for the interconnect, the optimum ratio between the radius of curvature and the length of the straight section could be determined by finding the minimum value of Eq. (24) in terms of R. Because of the complicated nature of this equation, this optimization would be quite laborious. However, in an extremely critical design it might easily be worth the time and effort.

Most previous work on interconnect design did not adequately treat the straight segments of the interconnect, as the following example shows. Using a radius of curvature of 0.025 m, different interconnect heights were obtained by lengthening the straight segments. The maximum bending stress was calculated for each interconnect, and the results are tabulated in Table 9. Each interconnect design used copper with a fatigue strength of 7750 N/cm². As can be seen, the minimum acceptable height is 1.016 cm. This example also shows that the Heliotek method is overly conservative. If necessary, a higher stress level could be tolerated, since the number of cycles is relatively low. The actual number can be calculated for the launch vibration conditions and the number of times the spacecraft will enter shadow during its lifetime. Based on this improved method of analysis, design situations will be better known and the ultimate strength of a material can be used without difficulty.

The values of Table 9 are shown graphically in Fig. 7.

Table 9. Maximum interconnect bending stress
($E_{copper} = 1.27 \times 10^7/cm^2$; $R = 0.025$ cm; $\sigma_{design} = 7750$ N/cm²; $\delta = 0.0013$ cm)

l, cm	$H = l + R$, cm	σ, N/cm²
0.000	0.025	42,977
0.025	0.051	14,496
0.051	0.076	7,415
0.076	0.102	4,544
0.119[a]	0.145	2,431
0.188[b]	0.213	1,198

[a]Corrected Heliotek design.
[b]Original Heliotek design.

V. Material Properties

Accurately known material properties are essential for the optimization of solar arrays since the design equations are no more accurate than the parameters within them. The following tables are a compilation of the presently available values of the parameters important to solar array design. Tables 10–14 deal with various adhesives used in
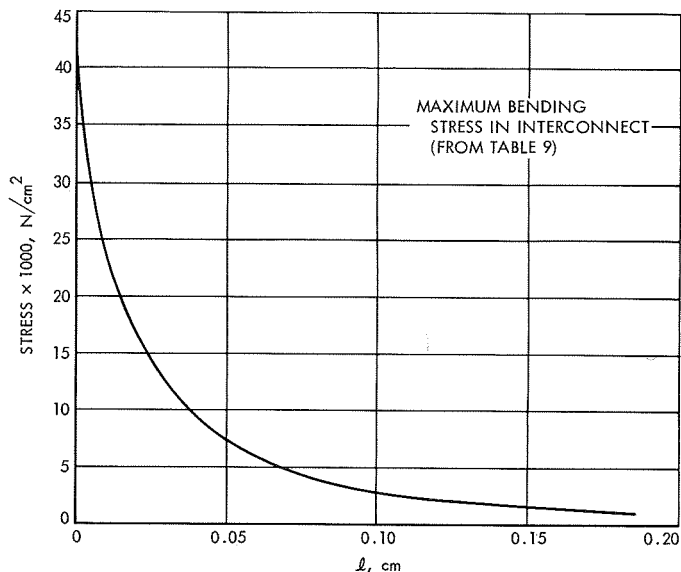
Fig. 7. Maximum bending stresses in interconnect (from Table 9)
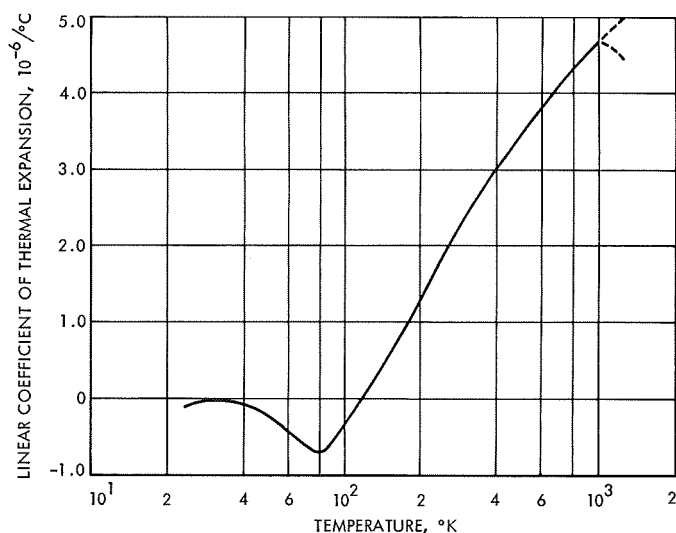
Fig. 8. Linear coefficient of thermal expansion in silicon

solar arrays. Table 15 covers the metals commonly used in solar arrays. Table 16 deals with the effect of temperature and crystal plane orientation on the coefficient of thermal expansion of silicon, while Fig. 8 is a graph of this temperature effect.

Tables 10 through 15 are from Ref. 6. Table 16 and Fig. 8 are based on data from Ref. 7, which is perhaps the best available source of information on silicon's properties. There is considerable information on the effect of crystal plane orientation on material properties. There is some

Table 10. Weight loss after exposure to pressures of 5×10^{-6} to 5×10^{-7} torr and temperatures of 93.3 to 121.1°C for 100 to 112 hours

Material	Mass before exposure, g	Mass after exposure, g	Mass loss, g	Mass loss, %	Observations
Flexible filled epoxy	26.557	26.290	0.267	1.01	No color change. Slight slump at bottom of sample
Flexible silicone	15.928	15.808	0.120	0.75	No color or dimensional changes
One component silicone sealant	3.936	3.734	0.202	5.13	No color or measurable dimensional change
Clear flexible silicone	13.400	10.098	3.302	24.64	Slight darkening and loss of 1.5 mm from the surfaces of the 2.54-cm cube
Modified dimethyl silicone	25.057	24.875	0.182	0.73	No color or measurable dimensional change
Phenolic rubber	4.3686	4.2668	0.1018	2.3	No color or measurable dimensional change
Epoxy polyamide	23.282	23.280	0.002	0.01	Slight darkening but no measurable dimensional changes
Polysulfide with chromate cure	14.610	13.641	0.969	6.63	Slight darkening. Sample bubbled and slightly expanded
Epoxy with anhydride curing agent	11.552	11.535	0.017	0.15	Slight darkening but no dimensional changes
Epoxy with amine hardener	9.937	9.719	0.218	2.2	No color or dimensional changes
Epoxy with Versamid hardener	8.964	8.646	0.318	3.5	No color or dimensional changes
Flexible epoxy with Versamid hardener	9.156	8.962	0.194	2.1	Both surfaces frosted. No dimensional changes
Polysulfide with lead oxide cure	15.617	10.354	5.263	33.70	Slight darkening. Sample bubbled and shrank approx 25%
Dimethyl silicone	16.237	16.105	0.132	0.81	No color or dimensional changes

Table 11. Comparative tensile strengths of adhesive-bonded aluminum specimens

Adhesive materials	Exposure conditions	Tensile average of five tests, N/cm^2	Adhesive materials	Exposure conditions	Tensile average of five tests, N/cm^2
Mylar tape with polyester adhesive on both sides	control, Tenney chamber	46.5 214.2	Dimethyl silicone with stannous octoate catalyst	control, Tenney chamber	43.0 40.9
Epoxy polyamide	↑	129.6 544.6	Phenolic rubber adhesive on a paper carrier	↑	34.5 35.2
Epoxy with an amine hardener		25.4 109.2	Mylar tape with rubber adhesive on both sides		35.2 33.8
Modified dimethyl silicone		143.7 149.4	Polyester film with phenolic rubber adhesive on both sides		46.5 54.3
Methylphenyl silicone		151.5 139.5	Fiberglass with silicone adhesive on both sides		9.2 16.9
Dimethyl silicone		110.6 108.5	Fiberglass with modified epoxy adhesive on both sides	↓	162.0 293.8
One-component silicone sealant	↓	5.3 9.1			
Glass tape with phenolic rubber, thermal setting, adhesive on one side	control, Tenney chamber	125.4 105.7	Fiberglass with epoxy adhesive on both sides	control, Tenney chamber	360.0 359.3

Tenney chamber: pressure of 5×10^{-6} to 1×10^{-8} torr and temperatures of 93.3 to 121.1°C for 100 to 110 h.

Table 12. Properties of coverglass adhesives

Property	Material				
	RTV-602	RTV-615	Sylgard 182	Sylgard 184	Dow Corning 93-500
Color	Colorless	Light straw	Light straw	Light straw	Colorless to light straw
Specific gravity	0.995	1.02	1.05	1.08	1.08
Durometer, hardness, shore A	15	35	40	40	
Viscosity (poises)	0.8–1.5	3.5	55	55	80
Thermal conductivity, cal-1 cm/1°C/s			5×10^{-4}	3.5×10^{-4}	3.5×10^{-4}
Coefficient of expansion, in./in./1°C			300	300	300
Refractive index	1.406	1.406	1.430	1.430	
Tensile bond strength, N/cm^2		564–705	564	423	557

Table 13. Properties of solar panel adhesives and primers

Property	Adhesives		Primers		
	RTV-40	RTV-41	SS-4044	Dow Corning 1200	SS-4004
Specific gravity	1.35	1.31	0.85		0.85
Viscosity (poises) at temperature	300–600	350–500		0.01	
Durometer, hardness (shore A)	55	50			
Tensile strength, N/cm^2	388	352			
Elongation, %	120	200			
Color	White	White	Clear	Red	Fluorescent pink

Table 14. Properties of conductive adhesives

Property	Material				
	Eccobond solder 56C	Eccobond solder 57C	Eccobond solder 58C	Eccobond solder 70C	Eccobond solder V-91
Temperature range of use, °C	−21.1 +176.66	−21.1 +176.66	−18.88 +260	−21.1 +148.9	−10 +148.9
Bond shear strength, N/cm^2	317	352	1127	705	352
Flexural strength, N/cm^2	8595	7186	6834		
Volume resistivity, ohm/cm	$<2 \times 10^{-4}$	$<6 \times 10^{-4}$	$<2 \times 10^{-3}$	$<2 \times 10^{-3}$	$<2 \times 10^{-3}$
Thermal conductivity, cal/cm^2/cm/°C/H	>0.652	>0.652	>0.652	>0.652	

Table 15. Physical and mechanical properties of metals used in solar cells

Property	Metal										
	Al	Ti	Ni	Cu	Mo	Pb	Ag	Sn	Au	Kovar[a]	Si
Specific weight, kg/cm^3	0.003	0.005	0.009	0.009	0.010	0.011	0.011	0.006	0.019	0.008	0.002
Coefficient of thermal expansion, cm/cm/°C	23.0	4.67	13.3	16.5	4.90	29.0	17.0	23.0	14.2	5.0	3.0
Thermal conductivity, cal/sq cm/cm/°C/s	0.57	6.6	0.22	0.941	0.34	0.083	1.0	0.15	0.71	0.40	0.20
Electrical conductivity, % IACS[b]	64.9		25	103	34	8.3	106	15.6	73.4		
Electrical resistivity, ohm cm	2.65	42	6.84	1.67	5.2	20.6	1.59	11.0	2.19	49	10
Magnetic susceptibility, 10^{-6} cgs	0.6	−3.17		−0.08	−0.93	−0.01	−0.02	−0.03	−0.15		−0.13
Modulus of elasticity, 10^6 N/cm^2	6.3	11.8	21.1	11.3	33.1	1.4	7.8	4.2	7.8	21.1	11.5
Specific stiffness, E/P × 10^6 cm	233.68	261.62	236.22	125.48	322.58	12.45	73.66	73.41	40.13	252.22	495.30
Tensile strength, 10^3 N/cm^2	4.8	24	32.4			1.3	12.8		13.4	54.6	
Yield strength, 10^3 N/cm^2	1.2	14.1	6.0			0.6	5.6		28.2	41.9	
Elongation, %	60	54	30			30	50			16.8	

[a]Kovar is not a pure metal, but rather an alloy of the following composition: 29 Ni, 17 Co, 53 Fe.
[b]International annealed copper standards.

information available regarding mechanical properties such as tensile and shear strength, but these values are for specialized cases and are not representative of the values for actual solar cells. The best way to determine these properties is to run careful laboratory tests on actual solar cells. This type of work is planned for the continuation project outlined in Appendix A.

It is important to do experiments on actual hardware and to use the data whenever possible, since these values will be much more realistic. Similarly, material and mechanical properties should be measured over the entire temperature range to be encountered during space operation.

Table 16. Coefficient of thermal expansion of silicon

Temperature range, °C	111 orientation	110 orientation
50–100	2.5	2.7
100–200	3.1	3.0
200–300	3.5	3.4
300–400	3.9	3.8
400–500	4.3	4.1
500–600	4.7	4.4
600–700	5.0	4.5
700–800	4.9	4.5
800–850	4.6	4.3

VI. Test Procedures

A good testing program is an important aspect of solar array design. It allows the designer to verify his analysis and to check the actual performance of his hardware. In this work the designer will use two basic types of test programs. The first tests the general properties of the hardware; the second tests hardware ability to perform under flight conditions. These two types of tests require different experimental procedures. For general properties tests, the experiments should deal with one phenomenon at a time, and should approximate as closely as possible an analytic problem that can be used to analyze the results. For example, in tests to determine the maximum allowable bending stress of a solar cell, the easiest procedure would be to simply support two edges of the cell and not support the remaining two edges. The cell can be loaded either by a point, line, or uniform pressure load. The uniform pressure is the most realistic case, and can be achieved by hydraulic loading. If this is too expensive or otherwise impractical, the other types of loadings can be used. In these cases, however, one must remember not to generalize the test data to flight condition deflections, since the loadings are not the same. The results of all of these tests can be analyzed by applying Timoshenko's theory of plates and shells (Ref. 3) or using the tables given in Section III. It is important that the boundary conditions in the test situation be the same as in the analytic solution. For example, simply supported edges may or may not allow in-plane movement.

A currently used test rig is shown in Fig. 9 and the results of the tests in Fig. 10. This type of test is good for calculating maximum bending stress but should not be used for flight conditions deflections; as stated earlier this type of test does not properly simulate flight condition loading.

Another currently used test is the contact pull-strength test (Fig. 11), which has been used as an acceptable criterion for solar cell contacts. In this test the contact is pulled until it finally separates from the cell, with the breakaway load being given as the test result. There has been some question as to test validity, and the matter is presently under investigation at JPL. The results should be available shortly.

The second type of testing is flight condition testing. Since this type of testing is designed to simulate actual conditions, every effort should be made to insure that the test is as realistic as possible. Complete array hardware
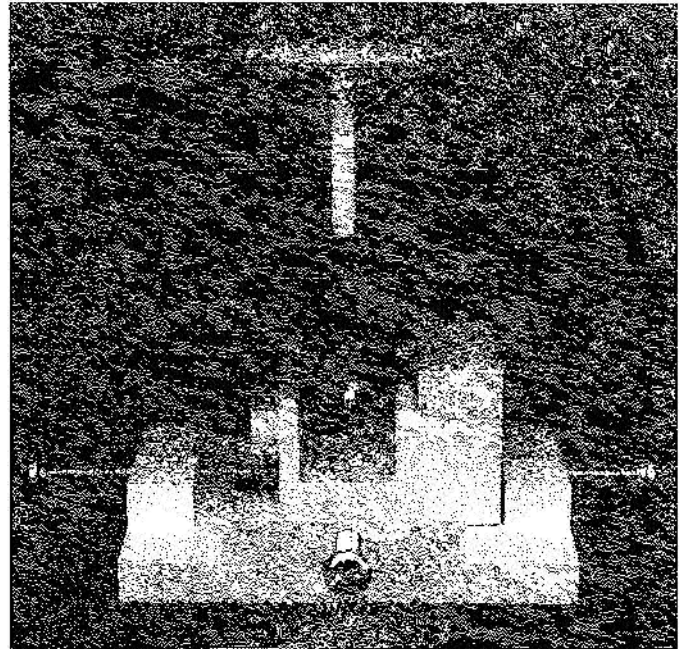
Fig. 9. Flexural strength test setup

should be used unless it can be shown that elimination of parts or the use of scaled-down hardware will not affect test results.

The two most common types of flight condition tests are thermal tests and shake tests. In the thermal tests the array is subjected to temperature extremes and shocks. As long as the cells have stress relief interconnects, small segment tests are acceptable. In all thermal tests the cells should be mounted on actual array substrate and the thermal gradients across the array thickness should be as realistic as possible. A thermal test setup is shown in Fig. 12.

Shake tests have usually been carried out on complete spacecraft. This procedure will probably have to continue, owing to the difficulty of matching natural frequencies and stiffnesses on scale models. If computer simulations are done, the ability of the cell and interconnect to withstand the maximum deflections could be tested on a smaller scale. It would be important to achieve the same radius of curvature as in the actual case; fatigue and acceleration loading tests would probably not be practical in this manner.

In general, then, tests of material or mechanical properties should be as simple and as pure as possible. If the desired results are hardware verification, the tests should be as realistic as possible.

44

SILICON SOLAR CELLS

CODE	MFG	LIGHT-SENSITIVE SIDE	SIZE, cm × cm-cm	PLATING	COATING (SiO)	SOLDER-DIPPED
A	RADIO CORP OF AMERICA	N	1 × 2-0.0457	Ti-Ag	YES	YES
B	HELIOTEK	N	1 × 2-0.0457	Ni	YES	YES
C	HELIOTEK	P	1 × 2-0.0457	Ni	NO	YES
D	TEXAS INSTRUMENTS	N	1 × 2-0.0355	Ti-Ag	YES	YES
E	HOFFMAN	P	1 × 2-0.0457	Ni	NO	YES
F	HOFFMAN	N	1 × 2-0.0457	Ni	NO	YES
H	RADIO CORP OF AMERICA	N	2 × 2-0.0203	Ti-Ag	YES	NO
J	RADIO CORP OF AMERICA	N	2 × 2-0.0203	Ti-Ag	NO	NO
K	HELIOTEK	N	2 × 2-0.0203	Ti-Ag	YES	NO
L	RADIO CORP OF AMERICA	N	2 × 2-0.0457	Ti-Ag	YES	YES
M	RADIO CORP OF AMERICA	N	2 × 2-0.0457	Ti-Ag	YES	NO
N	HOFFMAN	P	2 × 2-0.0457	Ni	NO	YES

GLASS FILTER COVERS

1   OPTICAL COATING LABORATORIES, 2 × 2 cm-0.0152 cm, 410 AR (ANTIREFLECTIVE)
2   OPTICAL COATING LABORATORIES, 1 × 2 cm-0.0152 cm, 410 AR (ANTIREFLECTIVE)
3   SAME AS ITEM 1 WITHOUT COATINGS

TEST CONDITIONS

1   SEMICLEAN ROOM
2   TEST APPARATUS: INSTRON MODEL TM-L AND CONTROL CONSOLE
3   CONSTANT LOAD SPEED: 0.01 cm/min
4   STRIP CHART RECORDER SPEED: 10 cm/min
5   RESULTS ARE BASED ON AVERAGE OF 2 SAMPLE/PLOT

LOAD, N
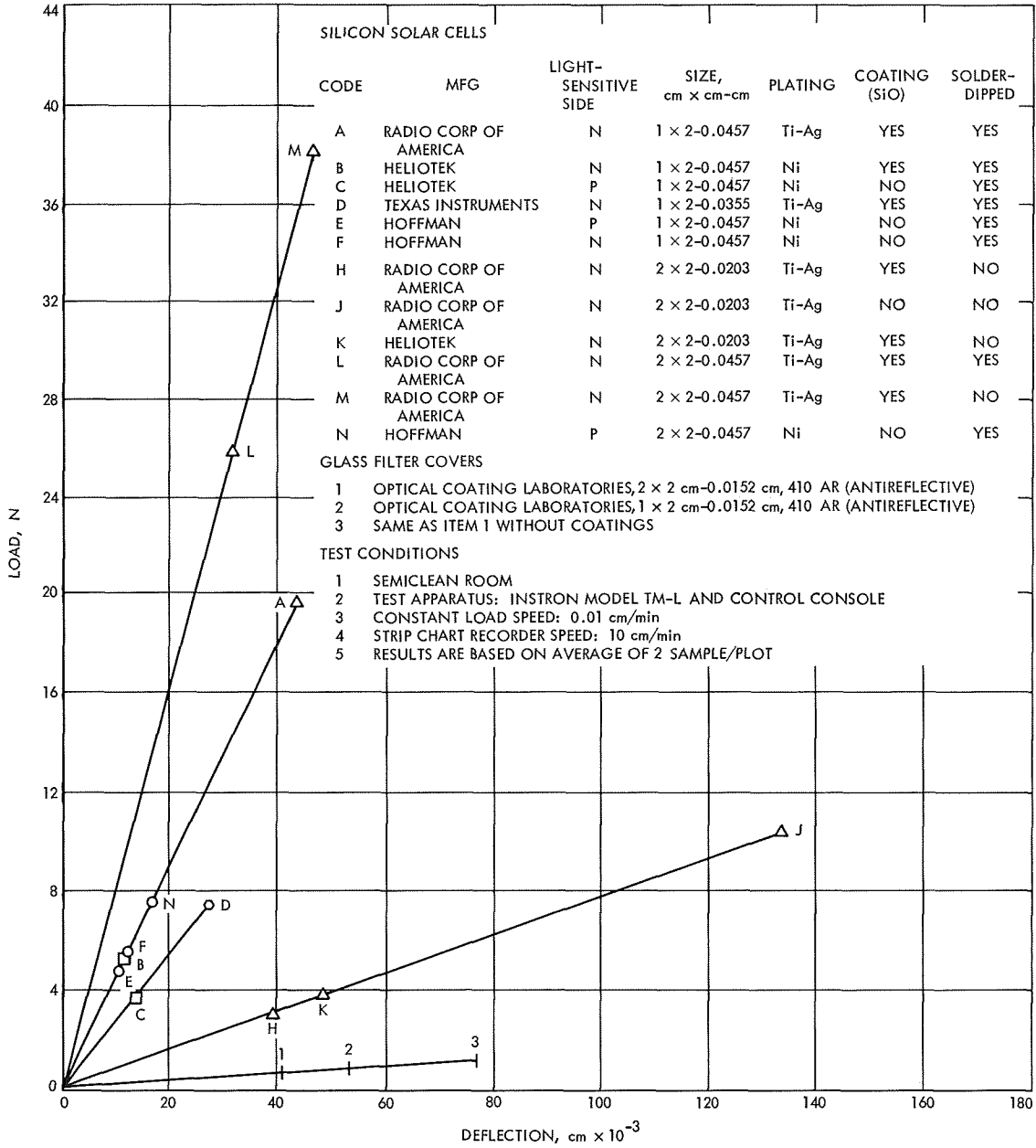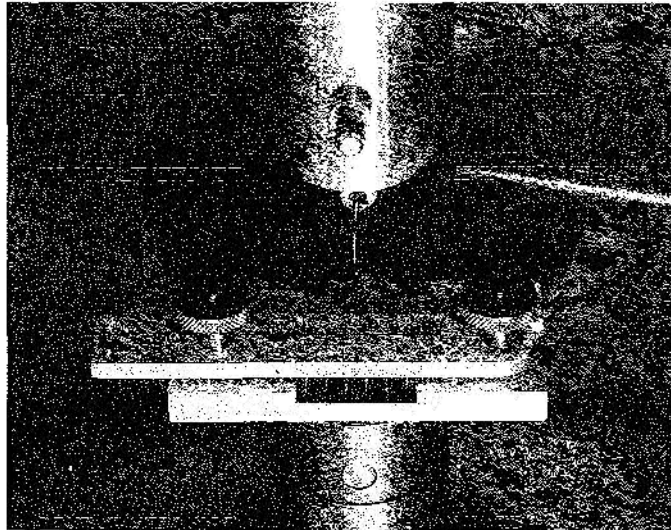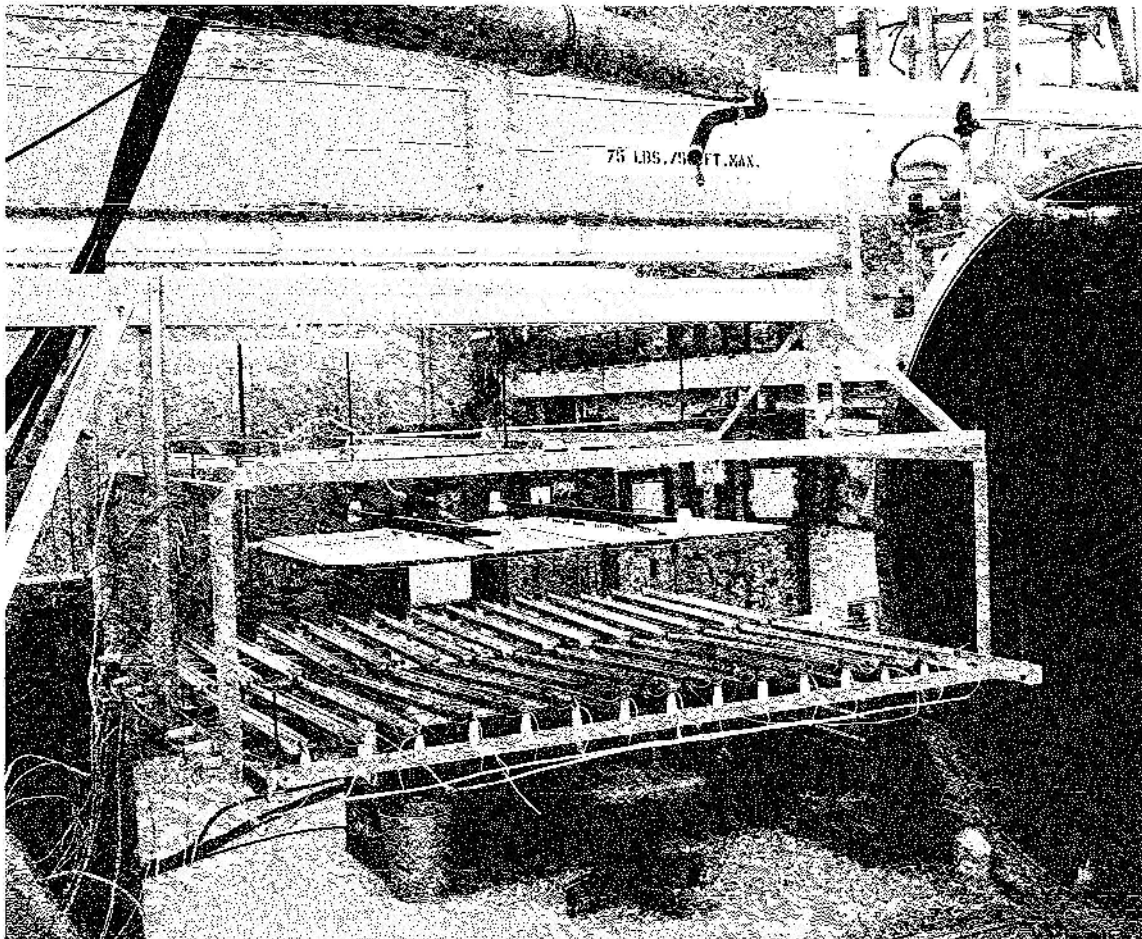
DEFLECTION, cm × 10^{-3}

Fig. 10. Flexural strength of silicon solar cells and coverglass

Fig. 11. Solar cell mounted in materials testing machine prior to contact strength test (note that thermocouple is positioned between cell and mounting fixture)

Fig. 12. Thermal test setup, actual array substrate

Appendix A

Study Plan: Structural Aspects of Solar Cells*

I. Solar Cell Stress Analysis

A. Evaluation of Various Cell/Interconnect Configurations

There have been numerous cell failures in the past in the area of the cell/interconnect interface. Attempts to explain these failures have been based on empirical tests of specific interconnect/cell configurations. The tests induced failures in the joint by simulating thermal shock or interconnect tensile load. The tests have served to improve designs mainly by indicating that the thickness of the interconnecting wire should be decreased. However, a more fundamental analytical approach is needed in order to be able to evaluate other current designs, proposed designs, or future designs. In addition, an analytical approach would represent an efficient method to introduce parametrical changes in any one of the designs after it was properly modeled. As an example, wire material, thickness, and width could be changed as well as solder thickness or even bond method; e.g., diffusion welding vs soldering. This analytical approach would model a slice through the thickness at the solar cell/interconnect interface. This model would be comprised of small rectangular and triangular platelets connecting a gridwork of nodes. The SAMIS computer program would be used. Specific tasks to be performed are as follows:

(1) Model present solar cell configuration on the SAMIS computer program and solve for stress pattern in cell/interconnect area due to different loading conditions.

(2) Vary parameters of the modeled cell/interconnect area to optimize design by minimizing stresses.

(3) Model the advanced cell/interconnect designs as currently being proposed by various industrial sources.

(4) Evaluate these designs on the basis of least-stress concentration due to applied loadings (both thermal and static).

B. Stress-Strain and Thermal Material Property Tests

A detailed analysis of the stress field in a solar cell due to static, dynamic, or thermal loading is highly dependent on reliable material properties. These values must also be known to properly evaluate the various qualification tests. It is therefore essential that the current condition,

in which there is a general lack of good physical properties, be corrected. The material properties that are needed are basically of two kinds, stress-strain relationships and thermal properties. It is proposed that the following tests be run to obtain thermal/physical properties on actual solar cell material:

(1) Thermal property tests to include specific heat, heat conductivity, and diffusivity at room temperature.

(2) Thermal property tests to include specific heat, heat conductivity, and diffusivity at different temperatures (within $\pm 150°C$).

(3) Stress-strain tests to include elastic moduli, Poisson's ratio, and stress-strain curves to failure at room temperature.

(4) Stress-strain tests to include elastic moduli, Poisson's ratio, and stress-strain curves to failure at different temperatures ($\pm 150°C$).

(5) Tests to determine whether thermal/physical properties are a function of crystallographic orientation.

C. Correlation of Pull Tests to Solar Cell Structural Integrity

It is common to require a pull test on a sample batch of solar cells. This pull test is accomplished by applying a load to a specified test tab soldered to the cell. The load is applied directly to the tab (bent perpendicular to the cell) so that the applied load tends to peel the tab off the cell. A value of this pull strength generally accepted as adequate has been established for specific designs by empirical tests. However, this practice leaves two areas of uncertainty: (1) there is no way at present to correlate the magnitude of the tab loading with the stress field in the cell; (2) there is no way to apply acceptable tab load values from one design concept to another. Hence it would be profitable to perform a stress analysis of the tab/cell interface under the loading conditions of the pull test. Since pull test data is available for the current JPL cell/interconnect design, a good check between analysis and actual samples is possible. The analysis could then be extended to other modifications of the current

---

*This appendix presents the project proposal for the current study program.

design or to entirely different designs. Specifically, it is proposed to:

(1) Modify the cell/interface model described in Section A to account for the bent tab.

(2) Perform stress analysis of the tab/cell interface under loading conditions of the pull test.

(3) Correlate stress analysis with the results of the pull tests from actual samples.

(4) Extend the analysis to cover other tab/cell configurations.

D. Establish Design and Acceptance Criteria

After performing the foregoing stress analyses, test evaluations, and material property generation for the solar cells under static and thermal loading, a set of design criteria for the solar cell structure will be established which will provide guidelines as to how best to design cell/interconnect junctions. It will also provide guidelines as to recommended pull test levels for cell acceptance.

II. Solar Cell Fracture Analysis

A. Experimentally Determined Fracture Properties

Since the materials used for solar cells are brittle in nature and also since each cell may contain external defects or internal flaws, cracks and impurities, the concept of fracture mechanics is very suitable for the fracture failure analyses of the cell. Basically, fracture mechanics is concerned with the propagation of existing crack-like flaws imbedded in materials or notch-like defects on the surface of the body. This information is directly related to the strength or performance of the cell material because all solid bodies contain cracks and flaws of different sizes, shapes, and orientations, internally as well as externally. It is assumed that fracture of a material is initiated by the propagation of an existing crack or flaw with either a critical size or an unfavorable orientation under a given loading condition.

To apply brittle fracture theory, it is first necessary to theoretically determine the stress intensity factor K, which depends upon the geometry of both the body and crack as well as the magnitude of the applied loading. This dependence is obtained from an elastic stress analysis.

To predict failure, the critical value of this stress intensity factor must be known. This critical value of the

stress intensity factor K_c (often called fracture toughness) is a material property and must be measured experimentally. To determine the value of K_c from a meaningful experiment is important; without the knowledge of the fracture property of the material, fracture analysis cannot be done.

The K_c value actually varies in different environmental conditions just like other material properties. Therefore it is not only necessary to measure the K_c value under one environmental condition but to perform a number of tests in a variety of test environments. The proposed test program on the determination of fracture properties is as follows:

(1) Fracture bending test of the precracked specimen at room temperature.

(2) Fracture bending tests of the precracked specimens at different temperatures ($\pm 150°C$).

(3) Fracture bending tests of the precracked specimens at different environments (such as vacuum).

B. Investigation of Fatigue Effect on Subcritical Flaw Growth of Solar Cells

Previous failure reports on solar cells show that a large amount of cells fractured when subjected to thermal cycling load. Thus it is worthwhile to examine the growth rate of subcritical cracks or other types of flaws in solar cells under cyclic loading. Experimental studies need to be conducted to determine how existing, but subcritical, cracks grow when subjected to low-level cyclic stresses. This knowledge is necessary to understand how small and unimportant flaws might increase until they reach critical size and cause complete fracture. The experiment approach proposed here includes:

(1) Determination of the relation of the crack size growth rate da/dN to various parameters including the range of the stress intensity factor ΔK, the mean value of stress intensity K_m, the loading frequency, and the stress condition (plane stress vs plane strain). The test will be conducted under room temperature conditions.

(2) Repetition of the tests under several extreme temperature conditions ($\pm 150°C$).

(3) Repetition of the tests under other various environmental conditions (vacuum, etc.).

C. Fracture Analyses

Fracture analyses on solar cell structures can be grouped into two categories:

(1) Analyses of external defects including defects on surfaces and edges of the cell and bonds between cell and coverglass and substrate. Analysis will be made of the studies of the various types of defect as well as their sizes and orientations subjected to the possible loading conditions, including static and dynamic loadings, thermal shock, and cyclic loading.

(2) Analyses of internal defects such as voids and impurities. The loading conditions will be static and dynamic loadings, thermal cyclic loadings, and shocks.

D. Statistical Analysis

Because the microstructure of real materials is not homogeneous, fracture initiation is a highly localized phenomenon, and material used for solar cells is in single-crystal structure, fracture phenomena of the solar cell structure lack good repeatability.

The wide scatter of the results of test is thus expected, and the nature of the observed scatter must be analyzed by statistical methods. The statistical approach to brittle fracture is concerned with two problems: the distribution function of brittle fracture strength of nominally identical specimens under nominally identical conditions, and the effect on brittle structure of specimen size, stress distribution, and state of stress. These problems are interrelated and their solution requires the construction of plausible physical-statistical models of the fracture process.

For the truly brittle material used for solar cells, the classical bundle model produces a Gaussian distribution, which will be used here. This distribution will provide the best representation of the fracture phenomena and the most reliable basis for extrapolation.

E. Establishment of Design and Acceptance Criteria

After performing fracture tests and analyses for solar cells under static and cyclic loading in various environmental conditions (temperature, vacuum, etc.), a set of design criteria for the solar cell structure will be established which will provide guidelines relative to the concepts of modern brittle fracture mechanics.

The manufacturers' acceptance criteria will also be established insofar as the defects of the cell are concerned. With knowledge of the fracture properties of the cell material and the fracture analyses, critical sizes of various defects under the dominant loading condition can be determined. From this information the criteria of acceptance for quality control can be established.

Appendix B

Proposed Study of Structural Aspects of Solar Cell Mechanical Tests*

I. Introduction

A solar array consists of a number of electrically interconnected solar cells mounted on a structural system designed to support the cells and their interconnections in some prescribed geometric orientation. There are several possible modes or types of interactions between the solar cells and the array structure. First, the mass associated with the cells and their interconnections may be a significant part of the total array mass. Thus the structure will be subjected to inertial loads associated with this mass. Second, for some constructions the stiffness associated with the cells and interconnections may contribute significantly to the overall array stiffness. Third, array structural deflections may produce significant stresses in the cells or interconnections. Fourth, the cells and interconnections may contribute significantly to the overall structural damping of the array.

Development efforts during the past few years have been directed toward producing very lightweight (i.e., high power-to-weight ratio) solar arrays. Most activities in this area have resulted in arrays with the solar cells and interconnects constituting a larger portion of the total array weight than was the case for earlier arrays. Thus the first-mentioned solar cell/structure interaction effect has been directly accentuated. The other interaction effects may also be accentuated in these lightweight array concepts.

Although the general nature of the above-listed interaction effects has been recognized for a long time, apparently little has been done to establish quantitative criteria, guidelines, or meaningful development test programs. In the development of new cell interconnect constructions, tension and peel tests are often performed; however, the results of such tests, although quantitative, can be related to structural adequacy only qualitatively. It would be very desirable to establish mechanical test programs, to be carried out during the development of solar cell constructions, which would provide more quantitative evaluations of the structural adequacy of proposed concepts. The study proposed herein would be directed toward (1) determining whether such test programs would be meaningful, (2) establishing the nature and extent of testing required, and (3) establishing a set of criteria or guidelines for relating test data to structural adequacy.

II. Proposed Study Program

Within these guidelines, this study program would be specifically concerned with the contacts, interconnects, busses, cell-coverglass attachment, cell-substrate attachment, and the cell stack as a unit. Previous tests on solar cells and arrays would be analyzed and the data consolidated and generalized where possible to establish trends as guidelines for future tests. It would also be desirable to establish guidelines concerning meaningful size and construction of test items: i.e., to ascertain to what extent single cell-contact tests are meaningful, or whether significant portions of an array structure must be included in the tests. Tests would be set up to analyze each area of concern with respect to imposed thermal, vibrational, impact, and inertial stresses and fatigue. The effects of both temperature extremes and thermal shocks would be considered. Interconnects and contacts would be analyzed for electrical as well as structural adequacy, as power losses may become significant before the minimum structure size has been reached. Special consideration will be given to the effects of coverglass and cell thickness on structural adequacy, since the trend has been toward thinner cells. Different array concepts and substrate materials would be analyzed as to their effect on the structural requirements of the individual solar cell. The requirements for the dielectric covering over a conducting substrate would be analyzed. Operating conditions would be set from foreseeable flight requirements (e.g., high-temperature requirements would be set from Venus-Mercury flight requirements). Structural tests and, ultimately, structural design criteria would be established if they are found to be meaningful. It is estimated that this program will require about 3 man-months of effort. In the event that highly meaningful results are obtained, it may be desirable to continue this program beyond its present scope.

---

*This appendix presents the original project proposal. Since it was written, there has been an increased emphasis on analytic techniques over the testing program. However, the general areas of concern are the same.

Appendix C

Solar Cell Interconnect Design and Analysis Symposium

On March 5, 1970, JPL sponsored a symposium on inter-connect design and analysis that was attended by representatives of manufacturers and users of solar cells. This appendix contains symposium presentations and a summary of the discussion.

I. Presentation by TRW Systems

A. Thermal Cycling Fatigue Stress Analysis on Solar Cell Interconnects

A theoretical study of solar cell thermal stresses was begun by TRW after observing failures in solar module extended thermal cycling tests. A rather unusual phenomenon was observed in that failures occurred only after several hundred cycles, clearly indicating a plastic-strain-related fatigue phenomenon rather than a simple exceeding of silicon tensile strength. Cracks were observed in the silicon at the toe of the interconnect solder joints. A stress analysis study determined the principal mechanisms leading to the failures and indicated the corrective action to be taken. This was subsequently verified by further thermal cycle testing.

An initial study was made using algebraic equations for thermal stress determination. This method, however, cannot accurately determine the high local stresses at the edges of interconnect joints and was abandoned in favor of more exact methods.

A two-dimensional finite-element computer program was utilized to develop the stress distribution through a cross-section of the solar cell and interconnect. The program operates by formulating a linear matrix representation of a triangular cross-sectional grid. The grid points (up to a maximum of 300) can be selected by the user to provide a fine mesh near discontinuities and a coarser mesh in the main portion of the cross section. Steep stress gradients can thereby be accurately developed.

Upon completion of the elastic thermal stress analysis, a low-cycle fatigue study was completed to predict the cycles to failure. This analysis was performed by converting the elastic stress into an equivalent total strain and comparing the plastic portion of the strain to the elongation of the material at temperature. Low-cycle fatigue life is related to the ratio of plastic strain to elongation.

The two-dimensional thermal stress analysis resulted in predictions of high solder stress with Kovar interconnects (force = 25,510–27,579 N/cm²; 37,000–40,000 psi) and relatively low silicon stress (δ < 6894.7 N/cm²; 10,000 psi). Fatigue life predictions on the order of 100 cycles is in fair agreement with test results. Slight variations in stress due to interconnect material and thickness change account for the significant change in percent failures due to statistical sensitivity of failures to stress level at high strains.

This study was directed at determination of stresses in the RTV bond attaching the cell to the substrate. Cracks and spalling failures at very low temperature soaks were noted in several cells around the periphery of the RTV. The analysis confirmed the presence of very high silicon stresses as the elastomer becomes stiff with decreasing temperature. The same two-dimensional finite element program was utilized to perform the stress analysis and to show the corrective action required.

B. Temperature Cycling Test on Module Assemblies

A series of engineering tests were performed to determine the ability of TRW's U-shaped solar module interconnect design and selected materials and processes to meet various long-term thermal cycling requirements. The tests were designed to demonstrate statistically significant differences in the test parameters. Typical test specimens were solar cell modules in a shingled configuration. Emphasis was placed upon determining the effect of different interconnect materials, interconnect thickness, cell adhesive patterns, and substrate materials upon solar module reliability through 300 thermal cycles. The temperatures ranged from 100 to −175°C and the rate of temperature change varied from 10 to 25°C per minute.

The interconnect materials investigated were copper, Kovar, and molybdenum. Interconnect thicknesses of 0.00254, 0.00508, and 0.00762 cm were evaluated. Test modules were bonded to magnesium, epoxyglass-faced aluminum honeycomb, and aluminum-faced honeycomb substrates using two different adhesive patterns. Interconnect-to-cell joining was accomplished using pulse-resistance and pulse-conductive soldering techniques.

Typically, electrical testing and microscopic examinations were performed at 0, 50, 100, 150, 200, and 300 temperature cycles. The appearance of microscopic cracks

around interconnect solder joints was found to be a sensitive failure criterion. The results showed that the interconnector material and substrate material should have a coefficient of thermal expansion similar to that of the silicon solar cell to survive extended temperature cycling. Also, the use of thinner interconnects reduces solder joint stresses caused by expansion and contraction of the substrate and results in a lower failure rate. The results of a design analysis indicated that the solder composition is an additional factor affecting long-term reliability. The solder fatigue failure rate was found to be strongly dependent upon stress level, in agreement with analytical predictions.

II. Presentation by Hughes Aircraft Company

Design, test, and analysis related to solar cell interconnects are taking an increasingly sophisticated approach. Kovar and molybdenum interconnects are preferred over copper for low-temperature applications because they approach the thermal coefficient of expansion of silicon. Kovar and molybdenum are popular and are in production use. There is a serious lack of materials properties at low temperature which are needed to perform meaningful stress analyses. Mission requirements will be more severe in the near future (longer life times, colder extremes for lightweight arrays, thinner and more fragile cells, etc.). Fatigue failures have been experienced where plastic deformation of solder or interconnect occurred.

Dimethyl silicones were initially selected by Hughes as adhesives. Later it was determined that flexible epoxy was better because of the crystallization shrinkage of the RTV. Current programs are employing RTV as well as the flexible epoxy.

Early solar cell module interconnects employed wires and tabs. Later, 0.0508–0.0762-mm-mesh copper was used. The Hughes cylindrical fiberglass panels are compatible with the epoxy bond and copper interconnects.

III. Presentation by Centralab*

Approximately two years ago, Centralab was faced with solar cell interconnector failures during temperature-cycling of the ISIS satellite solar panels. First attempts to resolve this problem were "shotgun" approaches, using several different materials on experimental panels. These experimental interconnects included various thicknesses

of copper, silver mesh with both orientations, and even platinum and other metals. All of these first experiments failed. Turning to a theoretical approach, we analyzed the interconnector as four little cantilever beams, each with one quarter of the deflection. (Total deflection throughout the temperature excursion is approximately 0.01778 cm.) The original interconnect of 0.00762-cm soft copper would have to withstand 206,842.7 N/cm² (300,000 psi) tensile stress if it was to remain in the elastic deformation range. This material is actually only capable of approximately 13,789.5 N/cm² (20,000 psi) before it yields. Under these conditions, most of the deformation was plastic flow, and the interconnectors were work-hardening to embrittlement in about 200 cycles.

To cure this problem, we first reduced the material thickness to 0.00254 cm. This automatically reduced the stress requirement to 68,947.57 N/cm² (100,000 psi). Next we increased the height of the interconnector expansion loop, which further reduced the stress requirement to less than 34,473.7 N/cm² (50,000 psi). The last design change was to fabricate the interconnectors of beryllium copper, heat-treated to a yield strength of approximately 75,842.3 N/cm² (110,000 psi). This left us an adequate safety factor. Experimental units were mechanically flexed the full 0.01778 cm thousands of times without any failure.

The problem of the interconnect-to-silicon junction is totally different. The stresses resulting from the differential thermal expansion of the interconnect and the silicon actually result in a shear loading at the interface. If the interface is composed of an elastomer as in the quartz-cover-over-silicon cell example, the shear loading in the elastomer may be presented as linearly increasing in intensity from zero at the center to a maximum at the outside edge. This is not the case however, when we analyze an interface composed of solder. The solder can elastically deflect only a fraction of that of the elastomer. In its resistance to deflection, it transmits significant tensile and compressive loads to the interconnect and the silicon. If we were to assume that the shear loading was increasing linearly with distance from the center, as in the case of the elastomer, it necessarily follows that the tensile/compressive loads would increase in a parabolic manner from zero at the outside edges to a maximum at the center. At the edges, where the shear load is the greatest, the tensile/compressive load would increase at the greatest rate. Near the center, where the shear load is small, the tensile/compressive load would hardly change. The tension/compression would be at the maximum in the center, being the sum of all the shear loads. If we are considering elastic deformation of the interconnector and

the silicon, it necessarily follows, from Hook's law, that the greatest incremental strain will be in the center, where the greatest stresses occur. At this point we see the fallacy of our assumption that the shear loading increases linearly as in the case of the elastomer. The change in shear loading must be the greatest where the tensile/compressive strain is the greatest. This results in a rapid rise in shear loading as we move away from the center, where the greatest tensile/compressive strain exists. The solution to these functions of shear and tension/compression must come from a simultaneous solution. In actual practice, we will find, however, that in the simple cooling down from the freezing point of the solder, the solder generally yields plastically due to overstressing. This redistributes the stresses and negates our preceding solution. The preceding solution is really not applicable anyway, owing to the fact that these thermal strains take place in all directions, and polar equations must be written from the centroid of the interface area. Centralab is presently working toward a solution to this entire problem.

In working with these interconnector stress analyses, we must be careful not to confuse tensile loads with shear loads. We must also remember that the failure stress levels under fatigue conditions are considerably lower than the failure stress under static loading. Another point at which some confusion has been noticed is that the proportionality of stresses with temperature for soldered joints must be related to the freezing point of the solder and not to some arbitrary temperature.

IV. Presentation by Heliotek*

A. Summary of Interconnector Design

Advanced silicon solar cell array designs have introduced new and unique problem areas in cell interconnector design. Two of these problem areas were selected for presentation at a JPL round table discussion held March 5, 1970. The two areas of concern are flexural fatigue of the solar cell interconnector during vehicle launching and deployment and retraction of the array and the interconnect stresses generated by the rapid thermal cycling as the array is alternately illuminated and shadowed. These are factors to be considered to upgrade solar power systems to meet new mission requirements.

A typical silicon solar cell array configuration with a conventional metal interconnector design is shown in

Fig. C-1. Redundant metal tabs are soldered to the top (negative) surface of a parallel group of cells. The interconnector has a stress loop formed in such a way that the interconnector passes between the parallel group of cells, thus completing the series connection of the array. Forces applied to a solar cell array are distributed between the substrate and the metal interconnections according to the spring rates K of the interconnector and the substrate. For conventional arrays, the substrate is usually a honeycomb structure made with a skin of aluminum 0.0254-cm thick. The more advanced designs utilize only a 0.00254-cm-thick polyimide film.

Any force applied to the array structure will be distributed in the ratio of the element spring rates. Therefore, in the aluminum substrate case, the force distribution will be:

$$\frac{K_i}{K_s} \cong \frac{1}{10}$$

So the substrate essentially carries the load. In the polyimide substrate case, the force distribution will be:

$$\frac{K_i}{K_s} \cong \frac{24}{1}$$

So the substrate stretches and distributes the load to the interconnect.

This last case is a highly undesirable situation since the ultimate loads for these thin interconnectors are low; additionally, it is an unreliable design in that it requires the member providing the electrical integrity to also provide the structural integrity. In order to minimize the problem, a stress-relieving loop is utilized in the interconnector so that the K_i is reduced to a negligible value. The size of
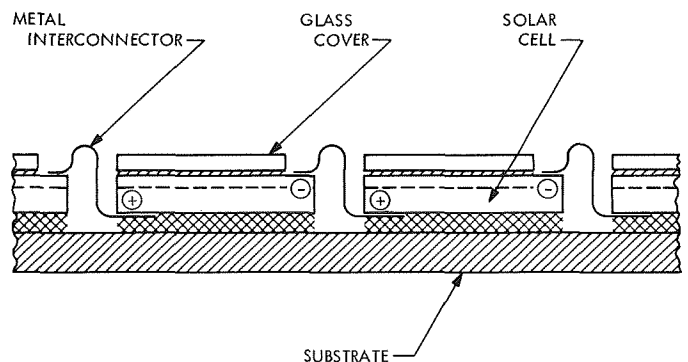

Fig. C-1. Solar cell interconnect design

the stress loop required will be dependent upon the inter-cell spacing change anticipated. The cell spacing will change as a result of applied forces during deployment, from thermal expansion, and from vibrational forces.

Thermal expansion effects can be described by one of two models shown in Fig. C-2. Case I is typical of the polyimide flexible substrate, where the cell is essentially rigidly bonded to the substrate and all thermal expansion effects on cell spacing are dependent upon the expansion of the region Y_1. Case II is typical of the aluminum rigid substrate, where the cell essentially "floats" with little rigidity between substrate and cell. The substrate expansion occurs with respect to the centroid of adjacent cells while the cell also expands; the intercell spacing change is the difference between the two. This model produces much greater intercell spacing changes. The calculation of the intercell spacing change ΔY is determined from the thermal expansion coefficient α of the materials and the appropriate temperature change ΔT. The calculated ΔY values then provide intercell spacing variations that would be expected owing to thermal changes and provide a minimum value for the length of the interconnector expansion loop. Empirically, thermal cycle tests have shown that this minimum interconnector loop is not satisfactory because of fatigue effects.

B. Stress Relief Loop Design

The stress relief loop must therefore be designed to account for the ΔY to prevent fatigue failure. For a given piece of material, the stresses incurred through bending are given by

$$S = \frac{Ex}{R}$$

where

E = the modulus of elasticity

x = the distance from the center of bending to the stress point in question

R = the radius of curvature

For a thin uniform interconnector, the center of bending will lie in a plane located midway through the thickness of the interconnector. Consequently, the maximum stress will be at the interconnector surface.

$$S_{max} = \frac{Ed}{R}$$
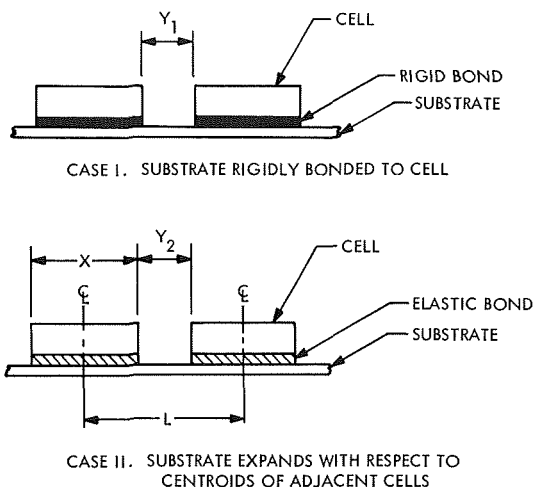
where d is half the thickness of the interconnector.

CASE I. SUBSTRATE RIGIDLY BONDED TO CELL

CASE II. SUBSTRATE EXPANDS WITH RESPECT TO CENTROIDS OF ADJACENT CELLS

Fig. C-2. Solar cell thermal expansion model

It is assumed that the interconnector stress relief loop was bent to its assembly shape and subsequently annealed or that the working was done so there was no residual stress. Stress will occur only with further bending. The maximum stress in the interconnector as a result of cell movement can be calculated as follows:

$$S_{max} = Ed\left(\frac{1}{R_i} - \frac{1}{R_f}\right)$$

where R_i and R_f are the initial and final radii of curvature.

A simple interconnect system which has essentially no expansion loop is schematically shown in Fig. C-3. However, there is a radius of curvature change that corresponds to the change in cell motion. The maximum allowable change in radius that will not make the interconnector exceed the endurance limit can be calculated as

$$R_f = \frac{R_i}{1 - \dfrac{S_f R_i}{Ed}}$$

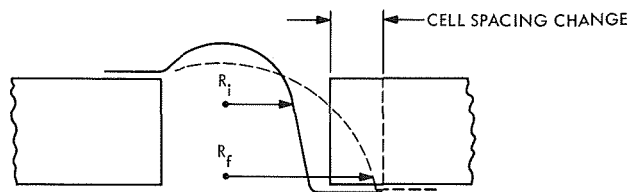where S_f is the "no-fatigue" stress level determined from appropriate tables or experiments.

Fig. C-3. Interconnect design with essentially no expansion loop

One way in which improved fatigue resistance can be obtained is to place the stress loop higher above the cell surface. In this type of design there will be less change in radius with linear cell motion. Figure C-4 schematically shows the impact of changing the interconnector height. The change in bend radius is significantly smaller than the change in cell spacing. The total loop height h' is defined as $h + R$, where R is the bend radius, ΔX is the change in bend radius that will fall within the endurance limits, Y is one-half the initial cell spacing, and ΔY is one-half the cell spacing change due to expansions. Then, from similar triangles,

$$\frac{X + \Delta X}{R} \qquad \frac{Y + \Delta Y}{h'}$$

Consequently,

$$h' = R\frac{\Delta Y}{\Delta X}$$

For no fatigue, then, the maximum allowable ΔX will be given by $\Delta X_{max} = R_f - R$.

All the variables in the equations above can be summarized as follows:

$$\Delta X = \left| R - \frac{R}{1 - \dfrac{S_f R}{Ed}} \right| = R \left| 1 - \frac{1}{1 - \dfrac{S_f R}{Ed}} \right|$$

and since $h' = R\,(\Delta Y/\Delta X)$ and substituting for ΔX above, then

$$h' = \Delta Y \left| \left(1 - \frac{1}{1 - \dfrac{S_f R}{Ed}} \right)^{-1} \right|$$

$$h' = \Delta Y \left| 1 - \frac{Ed}{S_f R} \right|$$

$$h' = \frac{\Delta Y'}{2} \left| 1 - \frac{Ed}{S_f R} \right|$$

where $\Delta Y'$ is the total cell spacing change.

Empirical tests where sample modules were subjected to motions which would induce interconnector flexing are summarized in Fig. C-5. The fatigue resistance of the high-stress loop over the low-stress loop is quite pronounced.
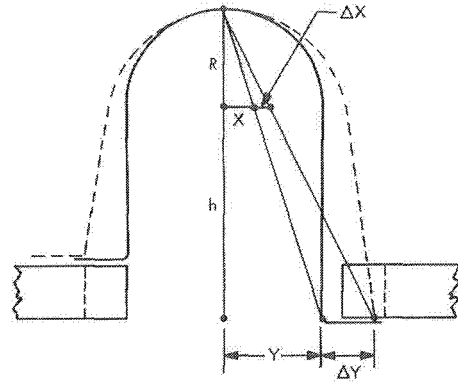

Fig. C-4. Interconnect design with expansion loop extending above cell surface

Other high-fatigue-resistant interconnector concepts are exhibited in the figure.

C. Thermal Expansion Stresses

The thermal expansion model for a system composed of silicon, solder, and an interconnector tab is shown in Fig. C-6. If the members were not mechanically coupled, thermal effects would cause each member to expand or contract to some "free" length ΔL. However, since these members are rigidly bonded together, they must all expand to the same length (assuming no bending), and the stresses are distributed within each member. The stress will be determined by the amount of deformation ΔX required to translate each member from the free expansion length to the actual expansion length R. The resultant length change is calculated by considering the weighted expansion as follows:

$$R = \frac{L\left(\sum\limits_{i=1}^{i=3} t_i E_i \alpha_i \Delta T \right)}{\left(\sum\limits_{i=1}^{i=3} t_i E_i \right)} = LR'$$

where

$t_i =$ the thickness of each member i

$L =$ the length of the members

$E_i =$ the modulus of elasticity

$\alpha =$ the coefficient of thermal expansion

$\Delta T =$ the temperature change

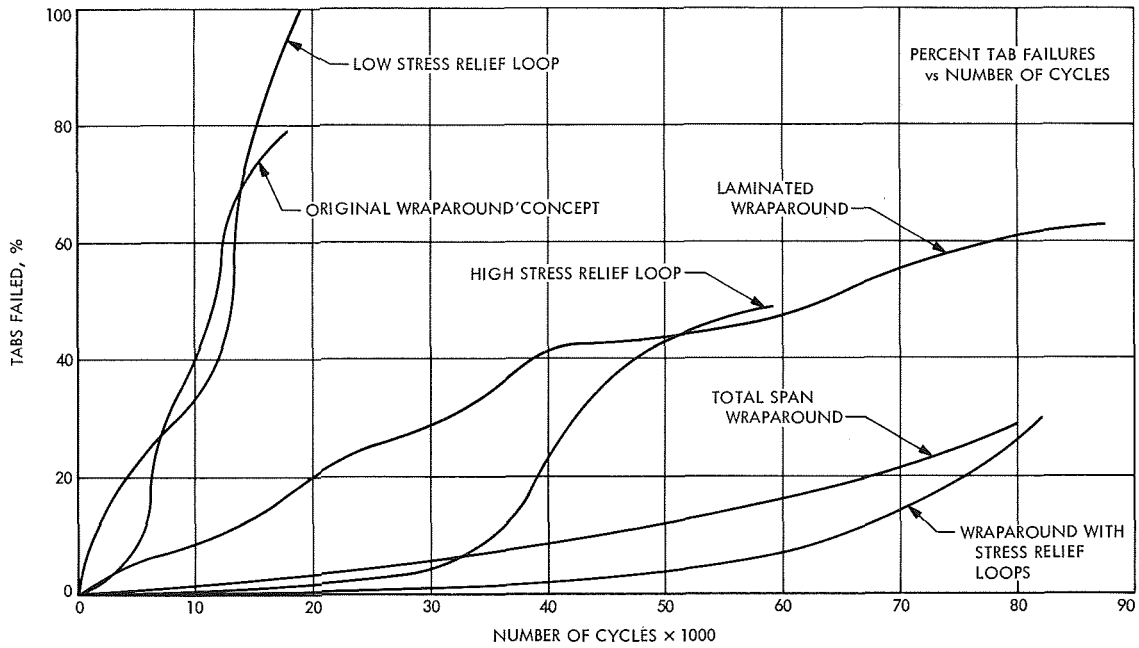$R' =$ the weighted mean of the length change
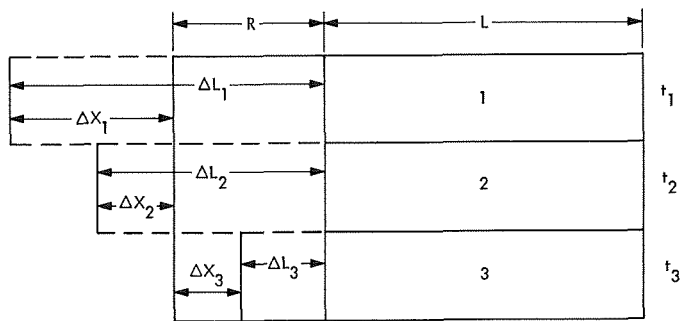
Fig. C-5. Flexure/tensile test

Fig. C-6. Thermal expansion model for a three-member rigidly bonded system

The strain induced in the member will then be:

$$\frac{\Delta X_i}{L} = \frac{\Delta L_i - R}{L}$$

$$= \alpha_1 \Delta T - R'$$

and the stress S_i in each member will be:

$$S_i = \frac{E_i \Delta X_i}{L} = E_i \left(\alpha_i \Delta T - R'\right)$$

Calculations were made to determine the stresses in the interconnector material, the solder layer, and the silicon cell using the above equation, but only the interconnector and solder stress values appear accurate using this model.

This analysis showed that the stresses in the solder were quite insensitive to interconnector material type and thickness. Therefore, empirical data was applied to a modified version of the model used above. In this modified model the thermal elongation weighted expansion value R' is determined by the total cell thickness, but the stress that would be calculated must be corrected by a stress concentration factor. This correction was determined empirically by taking the ratio of the fracture strength of silicon (19,200 N/cm²) to the calculated stress predicted by the model for a specific tab system which was known to cause silicon fracture at a certain temperature.

Figure C-7 shows the silicon stress for copper and molybdenum interconnectors when the temperature is reduced by an amount ΔT. Copper is a marginal design when a ΔT of 150°C or more is encountered. The advantage of using molybdenum or a metal with a similar thermal expansion coefficient as an interconnector is obvious under all conditions, but it becomes a necessity if reliable bonds are to be made that will survive very low temperature cycling.

D. Summary

Thermal expansion and vibrational motion of solar cells in an array are likely to cause stresses in the metal interconnectors sufficiently large so that fracture occurs. Interconnectors designed with a stress relief loop allow for cell motion. However, the bending will cause fatigue of the

metal if improperly designed. Generalized stress equations were developed that give the minimum stress relief loop dimensions for a "no-fatigue" interconnector. Also, the thermal expansion stresses induced at the metal-to-silicon interface were investigated and a generalized equation was developed for determining the stresses in each of the members. From these thermal expansion stress equations, it is possible to evaluate the effect of interconnector material and thickness on the stresses. These relationships can be used to determine the maximum allowable interconnector thickness that can be used without failure in thermal cycling environments.

V. Discussion Summary

The symposium was sponsored by JPL to determine (1) the current state of the art of solar cell interconnector design and analysis methods, and (2) what should be done in the future in this area. The major points brought forth were as follows:

Summary

(1) The most rigorous effect on solar cell interconnect design is due to the orbital temperature excursions of the solar array.

(2) Relatively little stress analysis and computer modelling has been done to date.

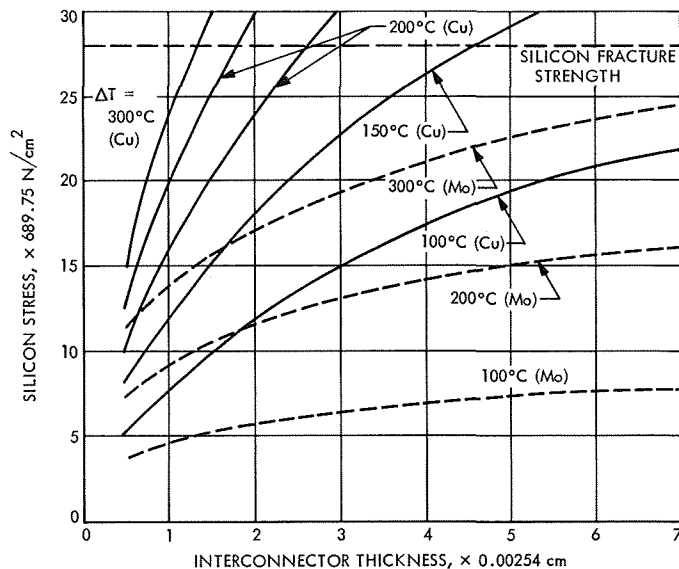(3) Before more valid analyses can be made, more detailed understanding of material properties must

Fig. C-7. Thermal stresses in silicon under a metal tab of various thicknesses

be obtained. Virtually no information is available for solar array materials at low temperatures.

(4) We need better, nondestructive test methods to determine the quality of interconnects and interconnect joints.

(5) Electrical performance testing alone does not insure quality of interconnects or interconnect joint integrity.

State of the Art of Analytical Techniques

(1) All interconnect designs in use to date have been developed by trial-and-error methods. Usually the only tests performed on a specific design were intended to demonstrate compliance with requirements. Design margins or ultimate design capabilities are generally unknown.

(2) Analytical stress models currently developed are highly oversimplified and represent actual designs only approximately.

(3) JPL presented a time-sharing computer program using a nonequal strain model for thermally induced variations in length. This model still uses linear coefficients of expansion and fully elastic material properties, but is a vast improvement over equal-strain models. Interesting curves presented were stress vs bond thickness/bond rigidity and bond thickness/bond rigidity vs substrate thickness.

(4) TRW presented an experimental parametric study of interconnect materials and thickness and a two-dimensional, linear, thermal elastic model for a finite element difference computer program (for adhesive between cell and substrate and for interconnects on solar cells). This model can treat silicon "scooping" underneath solder joints. The basic program is commercially available, but use is cumbersome.

Current Knowledge and Problems

(1) Heliotek showed that solder contact solar cells are no good for 10-yr missions on oriented lightweight arrays. Solder problem occurs at high temperatures due to fatigue; at low temperatures silicon cracks.

(2) Hughes had problems with RTV holding cells to substrates because of the anomalous volume expansion rate at crystallization temperatures. To circumvent these problems, flexible epoxies were developed and used on the ATS satellites. But recently,

RTV has again been used for more severe environments.

(3) Hughes used expanded silver plated copper mesh interconnects from 0.0508-mm stock, and rolled after expansion. These interconnects caused silicon "cratering" (local spalling) at low temperatures. Now they use etched copper grid mesh interconnects with wider openings.

(4) Hughes had difficulties in qualifying overseas solar cells. Structural integrity of domestic cells is far superior to that of foreign cells.

(5) Hughes currently develops special and unique beryllium-titanium skins for replacing fiberglass face sheets on honeycomb panels for advanced missions.

(6) Centralab has experienced failures in the expansion loops of expanded mesh interconnects due to temperature cycling. The problem was solved by making loops larger.

(7) Most stress analyses erroneously assume that a solder joint is stress-free at room temperature. In reality, zero-stress is encountered at solder freezing, and at room temperature yielding has already occurred. This yielding is the cause of early fatigue cracks.

(8) EOS has developed S-shaped interconnects. Those made from silver plated molybdenum have withstood 212 dips into LN_2 or about 1000 cycles between +71.1 and −73.3°C with a 90-min cycle. On 4- and 5-cell submodules assembled in tunnel oven, solder resist is used to control the solder area.

(9) Aerospace presentation showed that silicon solar cells will be required for at least another 10 yr. Therefore it is cost-effective to study stresses in the interconnects. Standardization of solar cells and solar arrays will play an important role in cost reduction. Solar cells in near-earth orbit require shielding for protection against proton radiation and weapons effects. The optimization of the latter requires the selection of low atomic number materials and the use of welded and plated interconnects.

Recommendations for Future Work

(1) Obtain temperature coefficients and stress/strain data on materials used on solar arrays, especially on the adhesives and silicon down to −180°C. Consider the nonisotropic behavior of silicon as well as effects of impurities and prestressed conditions due to manufacturing steps as well as the diffused layer.

(2) Expand present models to include nonlinear temperature coefficients, nonlinear stress/strain relationships, and elastic and plastic deformations.

(3) Expand models to analyze edge stresses at solder joints which lead to silicon "scooping" (local spalling).

(4) Include the following in the models:

(a) Material properties over broad temperature ranges.

(b) Substrate thickness and rigidity.

(c) Cell thickness and rigidity.

(d) Adhesive thickness (cover/cell and cell/substrate).

(5) Analyze ultimate stress cases as well as fatigue phenomena.

(6) Consider the following loads:

(a) Dynamic, due to vibrational launch conditions.

(b) Varying, due to roll-in, roll-out maneuvers.

(c) Static, due to temperature variations.

VI. List of Symposium Attendees

B. Anspaugh (JPL)
F. E. Beaumont (Xerox)
P. Berman (JPL)
D. Bickler (Centralab)
D. G. Cross (TRW)
W. C. Dunkerly (Hughes)
T. Eakins (Hughes)
G. E. Glattenberg (Heliotek)
J. V. Goldsmith (JPL)
W. Hasbach (JPL)
W. Jaworski (JPL)
K. Lui (TRW)
E. E. Maiden (TRW)
R. L. Mueller (JPL)

R. E. Oliver (JPL)
R. Opjorden (Hughes)
E. Ralph (Heliotek)
H. S. Rausenbach (TRW)
R. E. Ross (EOS)
R. G. Ross, Jr. (JPL)
L. Schmidt (JPL)
B. N. Smith (TRW)
P. M. Stella (Heliotek)
E. Stofel (Aerospace)
J. P. Thornton (TRW)
J. Weingart (JPL)
R. Wizenick (Xerox)
R. K. Yasui (JPL)

E. F. Zimmerman (Heliotek)

References

1. *Final Report*, Document 4039, prepared under JPL contract 952485. Electro Optical Systems (a division of Xerox Corp.), Pasadena, Calif., June 18, 1970.

2. Dietz, Albert George Henry, *Engineering Laminates*. J. Wiley, New York, 1949.

3. Timoshenko, Stephen, *Theory of Plates and Shells*. McGraw-Hill Book Co., New York, 1959.

4. *Standard Handbook for Mechanical Engineers*. Edited by T. Baumeister. McGraw-Hill Book Co., New York, 1969.

5. Seely, F. B., and Smith, J. O., *Advanced Mechanics of Materials*, Second Edition. John Wiley and Sons, New York, 1952.

6. *STOD Survey and Study for an Improved Solar Cell Module*, Section Report 900-270. Jet Propulsion Laboratory, Pasadena, Calif., Aug. 8, 1969.

7. Evans, R. A., et al., "Integrated Silicon Device Technology," *Physical/Electrical Properties of Silicon*, Vol. V. Research Triangle Institute, Durham, N. C., July 1964.

32

JPL TECHNICAL REPORT 32-1528
NASA — JPL — Coml., L.A., Calif.